https://doi.org/10.1093/plphys/kiac551 PLANT PHYSIOLOGY 2023: 191: 1416–1434

Plant Physiology®

Research Article

Ascorbate peroxidase 1 allows monitoring of cytosolic accumulation of effector-triggered reactive oxygen species using a luminol-based assay

Xiufang Hong [1], Fan Qi [1], Ran Wang[1], Zhiyi Jia [1], Fucheng Lin [1], Minhang Yuan [2], Xiu-Fang Xin [2] and Yan Liang [1,*]

1 State Key Laboratory for Managing Biotic and Chemical Threats to the Quality and Safety of Agro-products, Institute of Biotechnology, Zhejiang University, Hangzhou 310058, China
2 National Key Laboratory of Plant Molecular Genetics, CAS Center for Excellence in Molecular Plant Sciences, Institute of Plant Physiology and Ecology, Chinese Academy of Sciences, Shanghai 200032, China

*Author for correspondence: yanliang@zju.edu.cn (Y.L.)

X.H. and Y.L. planned and designed the research. X.H. performed most experiments. F.Q. helped with generation of *delt4* mutants. R.W. and Z.J. helped with cloning of *APX1*. F.L. was involved in planning and supervising the work. M.Y. and X.-F.X. helped with H_2DCFDA staining. X.H. and Y.L. wrote the manuscript.

The author responsible for distribution of materials integral to the findings presented in this article in accordance with the policy described in the Instructions for Authors (https://academic.oup.com/plphys/pages/General-Instructions) is Yan Liang (yanliang@zju.edu.cn).

Abstract

Biphasic production of reactive oxygen species (ROS) has been observed in plants treated with avirulent bacterial strains. The first transient peak corresponds to pattern-triggered immunity (PTI)-ROS, whereas the second long-lasting peak corresponds to effector-triggered immunity (ETI)-ROS. PTI-ROS are produced in the apoplast by plasma membrane-localized NADPH oxidases, and the recognition of an avirulent effector increases the PTI-ROS regulatory module, leading to ETI-ROS accumulation in the apoplast. However, how apoplastic ETI-ROS signaling is relayed to the cytosol is still unknown. Here, we found that in the absence of cytosolic ascorbate peroxidase 1 (APX1), the second phase of ETI-ROS accumulation was undetectable in Arabidopsis (*Arabidopsis thaliana*) using luminol-based assays. In addition to being a scavenger of cytosolic H_2O_2, we discovered that APX1 served as a catalyst in this chemiluminescence ROS assay by employing luminol as an electron donor. A horseradish peroxidase (HRP)-mimicking APX1 mutation ($APX1^{W41F}$) further enhanced its catalytic activity toward luminol, whereas an HRP-dead APX1 mutation ($APX1^{R38H}$) reduced its luminol oxidation activity. The cytosolic localization of APX1 implies that ETI-ROS might accumulate in the cytosol. When ROS were detected using a fluorescent dye, green fluorescence was observed in the cytosol 6 h after infiltration with an avirulent bacterial strain. Collectively, these results indicate that ETI-ROS eventually accumulate in the cytosol, and cytosolic APX1 catalyzes luminol oxidation and allows monitoring of the kinetics of ETI-ROS in the cytosol. Our study provides important insights into the spatial dynamics of ROS accumulation in plant immunity.

Introduction

Plants have evolved a sophisticated innate immune system as a protection mechanism against pathogen attacks. When pathogens reach the physical barriers on the plant surface, immunity-related responses are initiated by the cell surface receptor-mediated recognition of pathogen-associated molecular patterns (PAMPs), thereby activating PAMP-triggered immunity (PTI) (Boller and Felix, 2009; Zipfel, 2014; Bigeard et al., 2015). Through long-term interactions with their hosts, pathogens have evolved specific effector proteins. These are in turn recognized by intracellular nucleotide-binding, leucine-rich repeat receptors in plants, activating effector-triggered immunity (ETI) (Jones and Dangl, 2006; Wang et al., 2019; Ma et al., 2020).

Received May 18, 2022. Accepted December 2, 2022. Advance access publication December 3, 2022

Although PTI and ETI are initiated by 2 classes of receptors, they both use similar signals, including the influx of calcium, production of reactive oxygen species (ROS), and activation of mitogen-activated protein kinases (MAPKs) (Qi et al., 2011; Yuan et al., 2021b). Notably, PTI and ETI signals are mutually potentiated to activate strong immune responses to arrest pathogens (Ngou et al., 2021; Yuan et al., 2021a).

ROS are not only the by-products of normal metabolism during plant growth and development but also act as signaling molecules in response to many environmental stresses (Mittler et al., 2011; Suzuki et al., 2012; Baxter et al., 2014; Camejo et al., 2016; Mittler, 2017; Qi et al., 2017). Previous studies have reported biphasic ROS production in plants inoculated with avirulent bacterial strains; however, the kinetics of the 2 ROS bursts are very different (Doke, 1983; Baker and Orlandi, 1995; Lamb and Dixon, 1997; Mur et al., 2009). The first ROS peak within 1 h corresponds to PTI-ROS, whereas the second instance of ROS accumulation after approximately 8–24 h corresponds to ETI-ROS (Doke, 1983; Baker and Orlandi, 1995; Lamb and Dixon, 1997). Unlike most typical PAMPs, lipopolysaccharides (LPS), abundant in the outer cell envelope of gram-negative bacteria, trigger a biphasic ROS burst (Shang-Guan et al., 2018; Li et al., 2019, 2021; Wu et al., 2022). The transient first-phase ROS peak at approximately 0.5 h is similar to the PTI-ROS peak but much weaker than that induced by flg22 (a 22 amino acid peptide derived from bacterial flagellin). The strong second-phase ROS burst peaks at approximately 8 h and continues for several hours, a profile that bears an intense similarity to previous observations during bacteria-triggered ETI (Levine et al., 1994; Chandra et al., 1996; Shang-Guan et al., 2018; Li et al., 2021; Wu et al., 2022). Similar patterns of biphasic ROS production have been reported in plants subjected to free medium-chain 3-hydroxy fatty acids (e.g. 3-hydroxydecanoic acid, 3-OH-C10:0), identified as a contaminant in LPS preparations; however, the second peak occurs earlier and is lower than that induced by LPS (Kutschera et al., 2019; Li et al., 2021). Abiotic stresses, such as ozone and mild salt concentrations, can also trigger a biphasic ROS burst in Arabidopsis (*Arabidopsis thaliana*), in which ROS production reaches the first and second peaks at approximately 1 h and 6–18 h after treatment, respectively. In these biphasic ROS production patterns, the first peak is usually transient and rapid, whereas the second peak is slow and prolonged (Joo et al., 2005; Xie et al., 2011). In Arabidopsis, ROS production during an immune response is mainly mediated by the respiratory burst oxidase homolog D (RBOHD), a plasma membrane nicotinamide adenine dinucleotide phosphate (NADPH) oxidase (Torres et al., 2002). During PTI-ROS, RBOHD is activated by phosphorylation and the binding of Ca^{2+} and phosphatidic acid. This leads to the reduction of oxygen to superoxide, which is rapidly dismutated into hydrogen peroxide (H_2O_2) by superoxide dismutase (SOD) in the apoplast (Brandes et al., 2014; Kadota et al., 2014, 2015; Li et al., 2014, 2021). The ectopic expression of an avirulent bacterial effector enhanced the activities of key regulatory components of PTI-ROS and thus induced a long-lasting ETI-ROS burst in the apoplast (Yuan et al., 2021a).

Prolonged accumulation of H_2O_2 is toxic to cells. To avoid the toxic effects, all organisms contain a sophisticated system to detoxify oxidative stress, including enzymes such as ascorbate peroxidases (APX), catalases (CAT), and glutathione peroxidases (GPX), as well as a nonenzyme ascorbate-glutathione system (Apel and Hirt, 2004; Gest et al., 2013; Shigeoka and Maruta, 2014). APXs are mostly found in photosynthetic organisms, and different cellular compartments in plants contain their own APX isoforms, including cytosolic APX (cAPX), thylakoid membrane-bound APX (tAPX) in chloroplasts, stromal APX (sAPX), and microbody membrane-bound APX (mAPX) (Shigeoka et al., 2002). The different APX isoforms respond differently to metabolic and environmental signals (Caverzan et al., 2012). APX has a high specificity toward ascorbic acid as an electron donor and reduces H_2O_2 to water with the concomitant generation of monodehydroascorbate, a univalent oxidant of ascorbate that spontaneously disproportionates to ascorbic acid and dehydroascorbate (Smirnoff, 2000; Smirnoff and Wheeler, 2000). Cytosolic APX1 has been characterized as a central peroxidase that protects the chloroplast from oxidative stress (Davletova et al., 2005; Koussevitzky et al., 2008; Pandey et al., 2017). Under normal growth conditions, *apx1* mutants show retarded growth and reduced photosynthetic activity. Under high light, drought, and cold conditions, the leaves of *apx1* mutant plants show increased H_2O_2 accumulation, leading to reduced tolerance to these stresses (Davletova et al., 2005; Koussevitzky et al., 2008).

The study of ROS production is challenging because ROS are highly reactive and extremely unstable molecules. Therefore, the detection of ROS relies on measuring the end products formed when ROS react with specific probes (Zulfugarov et al., 2011; Griendling et al., 2016). Several colorimetric, fluorescent, and chemiluminescent probes have been developed to detect ROS production after treatment with immune elicitors or pathogens (Zulfugarov et al., 2011). 3,3-diaminobenzidine (DAB), which reacts with H_2O_2 to form a reddish-brown polymer, is a colorimetric probe typically used to detect H_2O_2, especially after infiltration with avirulent bacterial strains (Großkinsky et al., 2012; Kadota et al., 2019). Membrane permeable 2,7-dichlorodihydrofluorescein diacetate (H_2DCFDA) and membrane impermeable Amplex Ultra Red (AUR) are 2 fluorescent probes that are widely used in combination with confocal microscopy to visualize the spatial distribution of ROS (Ashtamker et al., 2007; Tian et al., 2016). Compared with colorimetric and fluorescent probes, chemiluminescent probes can interact with ROS and emit photons that can be detected by a luminometer or a sensitive CCD camera system (Khan et al., 2014; Yang et al., 2020). Most available luminescence detection systems are accompanied by a computerized system that allows continuous monitoring of the lights

emitted in response to various stimuli (Khan et al., 2014). Although the chemiluminescence method is not suitable for absolute quantitation of ROS production, it provides several advantages, such as the monitoring of ROS kinetics, imaging ROS production in vivo, and screening genetic mutants on a large scale (Dikalov et al., 2007; Khan et al., 2014; Smith and Heese, 2014; Griendling et al., 2016).

The most commonly used chemiluminescent probe is luminol (5-amino-2,3-dihydrophthalazine-1,4-dione), which emits light at a maximum wavelength of 425 nm when oxidized (Khan et al., 2014). Exogenous addition of peroxidases such as the frequently used and commercially available horseradish peroxidase (HRP) could enhance luminol oxidation (Coyle et al., 1986; Thorpe and Kricka, 1986). Luminol/HRP-dependent chemiluminescence assays have been widely used to study ROS kinetics in leaf disks after immune elicitor treatment (Smith and Heese, 2014; Sang and Macho, 2017). Although luminol is a small molecule that can cross plasma membranes, HRP cannot penetrate cell membranes; therefore, the luminol/HRP-based assay is typically considered to measure extracellular "oxidative bursts." Recently, this approach has also been used to measure the biphasic ROS burst (Shang-Guan et al., 2018; Ngou et al., 2021; Yuan et al., 2021a).

In this study, we monitored ROS production using a luminol-based chemiluminescence assay and found that Arabidopsis *apx1* mutants showed reduced long-lasting ROS accumulation in response to LPS, 3-OH-C10:0, and *Pseudomonas syringae* pv. *tomato* (*Pst*) DC3000 (*avrRpt2*). However, *apx1* mutants displayed increased ROS production when it was measured using DAB staining. Remarkably, we found that APX1 acts as a catalyst in the luminol-H_2O_2 reaction, and the W41F mutation in APX1 that mimics the critical residue of HRP enhanced its catalytic activity toward luminol. As APX1 is a cytosolic peroxidase, these results imply that sustained ETI-ROS might accumulate in the cytosol. Indeed, we did observe cytosolic accumulation of ETI-ROS in the cytosol when ROS were measured using DCF staining. Taken together, the in vivo catalytic activity of APX1 in the luminol-based chemiluminescence system reveals that ETI-ROS triggered by avirulent bacterial strains eventually accumulate in the cytosol.

Results

Arabidopsis *apx1* mutants show abolished long-lasting ROS production after LPS treatment

The long-lasting ROS bursts triggered by LPS, 3-OH-C10:0, and avirulent bacteria shared similar kinetics (Supplemental Figure 1). To investigate the molecular mechanism underlying the regulation of the long-lasting ROS burst, we first isolated mutants *defective in LPS-triggered ROS production* (*delt*) from ethylmethanesulfonate (EMS)-mutagenized Arabidopsis plants. The *delt4* mutants showed almost no long-lasting ROS production after LPS treatment (Figure 1A), whereas the transient ROS burst triggered by flg22 was slightly higher in *delt4* mutants than that in the wild type (Figure 1B). ROS production was monitored using a luminol-based chemiluminescence assay, and we found that the addition of HRP did not significantly promote chemiluminescent signals when flg22- and LPS-induced ROS levels were high enough to oxidize luminol to produce chemiluminescence (Supplemental Figure 2). Therefore, we did not add HRP in the following ROS measurement unless otherwise mentioned. The *delt4* mutant was backcrossed to the wild type, and the LPS-triggered ROS burst was evaluated in the resulting F_1 and F_2 populations. All tested F_1 plants ($n = 12$) showed a level of ROS similar to that of the wild type after LPS treatment. Among the 365 tested F_2 plants, 70 showed no second ROS burst after LPS treatment, whereas the others were like the wild type (with ROS: without ROS = 295:70, $\chi^2 = 6.6$, $P > 0.01$), indicating that the *DELT4* mutation is recessive in a single nuclear gene. The original *delt4* mutants were backcrossed with the wild type twice, and the homozygous progenies of F_3 or subsequent generations were used in all the experiments described below.

To genetically map *DELT4*, we generated an F_2 population derived from the cross between *delt4* mutants and the Landsberg *erecta* (Ler) ecotype. We roughly mapped *DELT4* to Chromosome 1 at a position between 2 molecular markers—F10K1 and F22O13—that are 0.57 Mb apart (Supplemental Figure 3A). We also identified single nucleotide polymorphisms (SNPs) in *delt4* mutants compared with the wild-type gene using bulked-segregant analysis. The F_2 progenies generated from the backcross between *delt4* and Col-0 were divided into 2 pools according to the mutant or wild-type ROS levels. Genomic DNA from 25 individuals was pooled and subjected to whole-genome sequencing (Supplemental Figure 3B). After filtering for detected SNPs, 2 nonsynonymous SNPs were found in the linkage region of the At1g07890 and At1g07700 genes (Supplemental Figure 3C). To identify which mutation caused the *delt4* phenotype, complementation tests were performed by transferring wild-type At1g07890 and At1g07700 to the *delt4* mutants. Accordingly, At1g07890 (encoding the APX1 protein) complemented the ROS levels in *delt4* mutants (Figure 1, C–E), but At1g07700 did not (Supplemental Figure 3D). The *delt4* mutant harbors a G-to-A mutation at nucleotide 1083 of *APX1*, which is the splicing site of the fifth intron (Figure 1C). To complement the *delt4* mutants, the genomic DNA of *APX1* was expressed under the control of the *APX1* native promoter in the *delt4* mutants background (referred to as *pAPX1::APX1/delt4*). In 4 independent transgenic lines, the LPS-induced ROS levels were rescued in *delt4* (Figure 1, D and E). Moreover, similar to *apx1-2* T-DNA insertion mutants, *delt4* showed significantly low levels of *APX1* transcripts and no detectable APX1 proteins (Supplemental Figure 4). Allelic tests conducted by crossing *delt4* to *apx1-2* indicated that they were allelic to each other (Figure 1F). Together, these results indicate that the reduced ROS levels in *delt4* after LPS treatment are caused by the mutation in *APX1*.

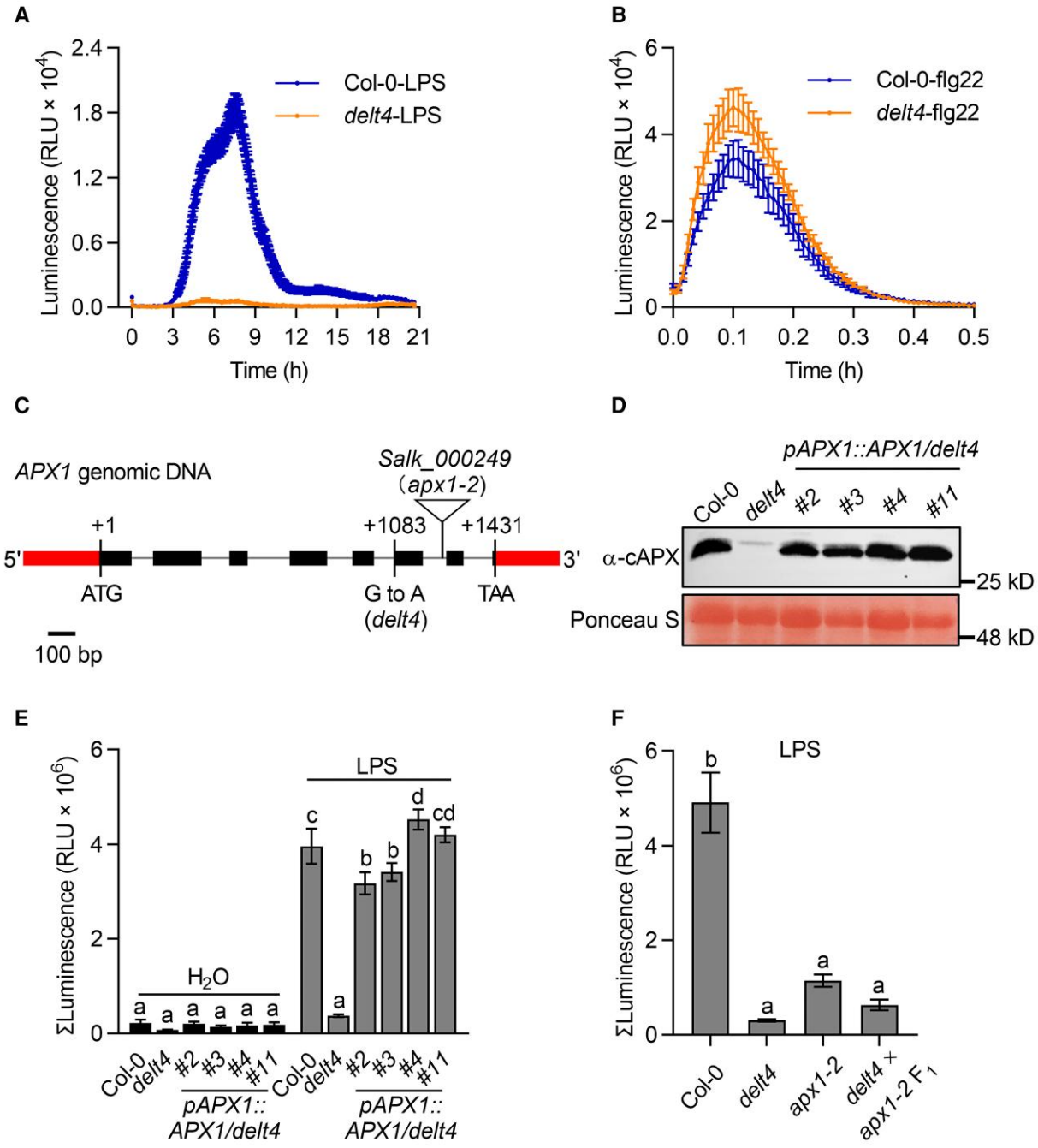

Figure 1 The *apx1* mutants show abolished long-lasting ROS signals after LPS treatment. A, The *delt4* mutants showed abolished long-lasting ROS signals after treatment with 50 μg mL^{-1} LPS. The dynamics of ROS signals were monitored for 21 h using a chemiluminescence assay with luminol as a substrate. Data are presented as the mean ± SE ($n = 16$). B, The *delt4* mutants showed increased ROS signals after treatment with flg22 (100 nM). The dynamics of the ROS signals were monitored for 30 min using a chemiluminescence assay with luminol as a substrate. Data are shown as the mean ± SE ($n = 6$). C, Schematic representation of the *APX1* gene. Mutations in the *delt4* and T-DNA insertion sites in the *apx1-2* are indicated. The start codon (ATG) and stop codon (TAA) are indicated. D, APX1 protein levels in 4 independent *pAPX1::APX1/delt4* transgenic lines. The genomic DNA of *APX1* was expressed under the control of the native *APX1* promoter in the *delt4* mutants background (referred to as *pAPX1::APX1/delt4*). Total proteins were extracted from 8-day-old seedlings and detected by immunoblot analysis using an α-cAPX antibody, and Ponceau S staining of the membrane served as a loading control. E, The *APX1* transgene complemented the ROS signals in *delt4* mutants. The bar graph indicates the total integrated photon counts within 1–21 h after 50 μg mL^{-1} LPS treatment. Data are presented as the mean ± SE ($n = 8$). Different letters above the bars indicate significant differences between the genotypes ($P \leq 0.05$, one-way ANOVA). F, *delt4* is allelic to *apx1-2*. F_1 plants were generated by crossing *delt4* to *apx1-2*. The experimental conditions were similar to those used in (E). Data are presented as the mean ± SE ($n = 8$–12). Different letters above the bars indicate significant differences between the genotypes ($P \leq 0.05$, one-way ANOVA). All experiments were repeated 3 times with similar results.

APX1 is required for the production of long-lasting ROS triggered by 3-OH-C10:0 and *Pst* (*avrRpt2*)

LPS preparations may be contaminated with 3-OH-C10:0, which also induces similar biphasic ROS production (Kutschera et al., 2019). Although the first transient burst triggered by 3-OH-C10:0 is stronger than that induced by LPS, the second sustained ROS peak occurs earlier at approximately 3–6 h but is much weaker than that induced by LPS (Supplemental Figure 1). Therefore, we also examined ROS production in *delt4* and *apx1-2* plants after treatment with 3-OH-C10:0. Similar to the response to LPS, samples from *delt4* and *apx1-2* plants showed reduced long-lasting ROS signals, but also showed an enhanced transient early ROS burst (Figure 2, A and B). Furthermore, we also examined whether APX1 is required for effector-triggered long-lasting ROS. Avirulent *Pst* (*avrRpt2*) bacteria activate resistance to *P. syringae* 2 (RPS2)-dependent ETI responses in Arabidopsis. We monitored the ROS production in leaf disks after incubation with avirulent *Pst* (*avrRpt2*) bacteria using a luminol-based chemiluminescence assay. The pattern of biphasic ROS production triggered by avirulent *Pst* (*avrRpt2*) bacteria is similar to that induced by LPS/3-OH-C10:0. The first ROS peak occurring within approximately 0.5 h corresponds to PTI-ROS, whereas the second kinetically slower ETI-ROS peak at 3–6 h after treatment lasts for several hours (Supplemental Figure 1). We found that the ETI-ROS signals were significantly reduced in *delt4* and *apx1-2* mutants compared with those in the wild type (Figure 2, C and D, Supplemental Figure 5, A–D). The *rbohD* and *rps2* mutants were used as negative controls for this experiment. High concentrations of bacteria ($OD_{600} = 0.3$ or 0.03) induced a strong early ROS burst, whereas the early transient ROS peak in *delt4* and *apx1-2* mutants was like that in the wild type (Figure 2C, Supplemental Figure 5A). When low concentrations of bacteria ($OD_{600} = 0.003$) were used, the early transient ROS peak was nearly undetectable while the long-lasting ROS peak was slower than that triggered by high bacterial concentrations (Figure 2C, Supplemental Figure 5, A and C). However, regardless of the bacterial concentration, the prolonged ETI-ROS signals were significantly reduced in *apx1* mutants (Figure 2D, Supplemental Figure 5, B and D). The addition of HRP slightly enhanced the luminescent signals in both wild type and mutants, but the decrease of luminescent signals in *apx1* mutants was similar to that without HRP (Supplemental Figure 6), suggesting that exogenous application of HRP cannot rescue the reduced ETI-ROS signals in *apx1* mutants, as monitored by a luminol-based chemiluminescence assay.

We also crossed *delt4* mutants with a transgenic line carrying dexamethasone (Dex)-induced expression of the bacterial effector gene, *avrRpt2* (referred to as Col-$0^{Dex:avrRpt2}$). Consistent with previous results (Yuan et al., 2021a), without the activation of PTI, Dex only induced a weak ETI-ROS burst (Supplemental Figure 5, E and F). Co-treatment with flg22 and Dex induced a strong ETI-ROS signal in Col-$0^{Dex:avrRpt2}$, whereas *delt4*$^{Dex:avrRpt2}$ showed almost no long-lasting signals (Figure 2, E and F). Collectively, these results suggest that *apx1* mutants show reduced long-lasting ROS signals triggered by 3-OH-C10:0 and an avirulent effector AvrRpt2, as monitored by a luminol-based chemiluminescence assay.

Loss of APX1 does not substantially enhance the expression of other H_2O_2-scavenging enzymes

As APX1 is an H_2O_2-scavenging enzyme, it is intriguing to observe a reduced long-lasting ROS burst in *apx1* mutants. However, the absence of *APX1* has been reported to elevate other H_2O_2-scavenging enzymes, such as CATs or GPXs (Jiang et al., 2016). Therefore, we compared the expression of transcripts encoding other cytosolic APX, CAT, and GPX enzymes involved in stress responses between the wild type and *apx1* mutants (Mittler, 2002). Our results indicated that these genes were not substantially altered in *apx1* mutants after LPS treatment (Supplemental Figure 7). Furthermore, *apx2*, *cat2*, and *cat3* mutants did not show altered long-lasting ROS production in response to LPS (Supplemental Figure 8). These results suggest that the reduced long-lasting ROS in *apx1* mutants is not due to elevated H_2O_2-scavenging enzymes. In addition, cytosolic APX1 is a central component that regulates redox homeostasis by protecting chloroplasts under abiotic stresses (Davletova et al., 2005). Therefore, we collected 4-week-old mature leaves 4 h after LPS treatment and compared the chloroplast structure between the wild type and *delt4* mutants under transmission electron microscopy. We found that the number and size of chloroplasts, plastoglobules, and thylakoids in *delt4* mutants were not considerable different from those in the wild type (Supplemental Figure 9A). In a previous study, we had found that the addition of LPS impaired chloroplast function in young seedlings, as evidenced by the release of green fluorescent protein (GFP)-tagged small subunit of ribulose-1.5-bisphosphate carboxylase (SSU-GFP) from the chloroplasts (Shang-Guan et al., 2018). Here, as ROS production was measured in mature plants, we re-evaluated the SSU-GFP release using 4-week-old leaves. We did not observe a substantial release of SSU-GFP from chloroplasts 4 h after LPS treatment, likely because of the stronger stress tolerance in mature leaves. Compared with the wild type, *delt4* mutants showed no obvious release of SSU-GFP from the chloroplasts, suggesting that *delt4* mutants did not exhibit considerable chloroplast dysfunction after LPS treatment (Supplemental Figure 9B). Taken together, these results suggest that the loss of APX1 function does not enhance the expression of other H_2O_2-scavenging enzymes or cause the dysfunction of chloroplasts.

Loss of APX1 does not affect the abundance of RBOHD

ROS production in plant immunity is mainly mediated by RBOHD; therefore, we compared the RBOHD levels between

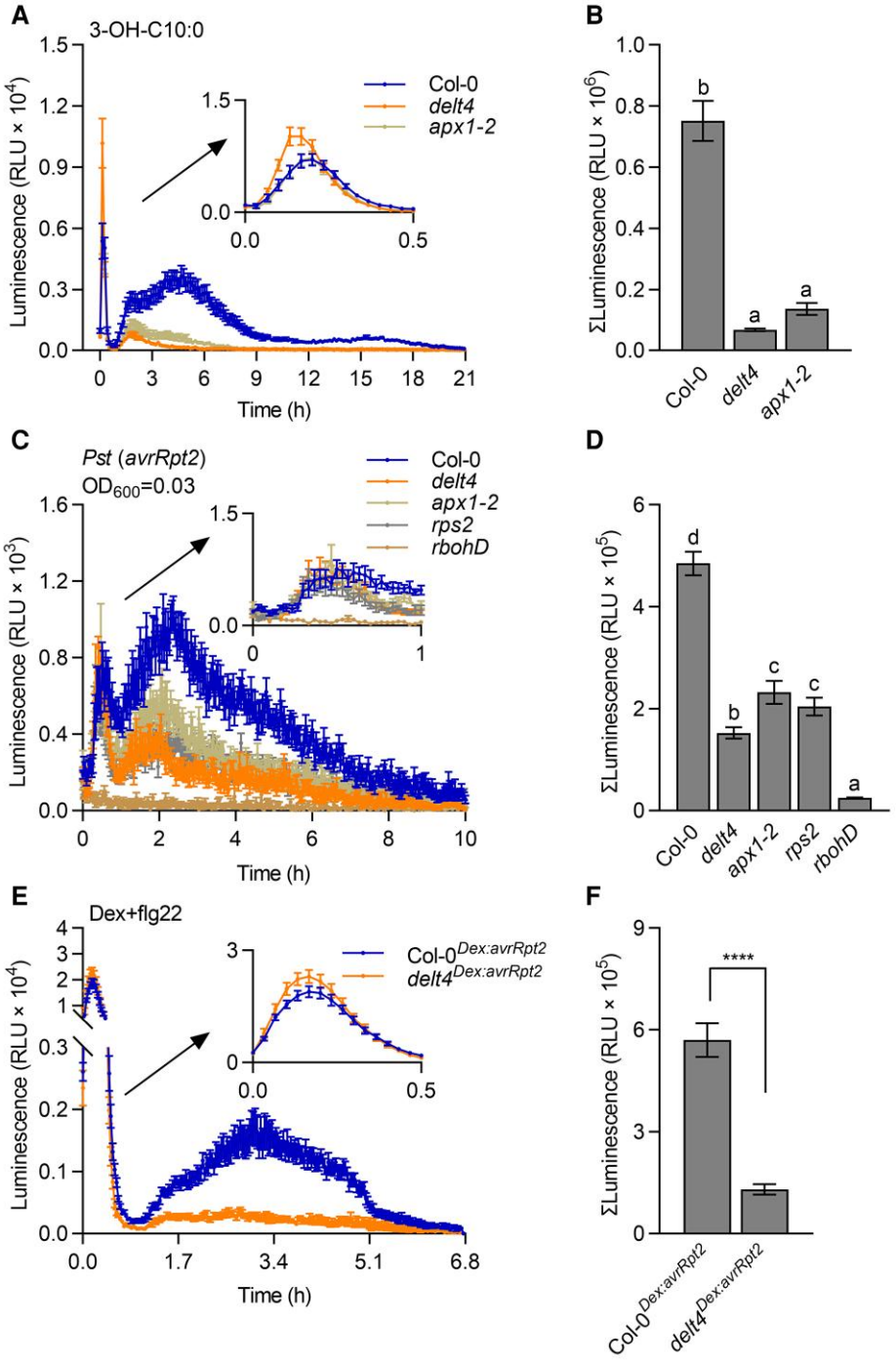

Figure 2 APX1 is required for the long-lasting luminol-based light signals triggered by 3-OH-C10:0 and an avirulent effector AvrRpt2. A, The *delt4* and *apx1-2* mutants showed reduced long-lasting ROS signals after treatment with 3-OH-C10:0 (5 μM). ROS signals were monitored for 21 h using a chemiluminescence assay with luminol as a substrate. Data are shown as the mean ± SE ($n = 16$). B, Total ROS signals within 1–21 h from (A). Data are shown as the mean ± SE ($n = 16$). Different letters above the bars indicate significant differences ($P \leq 0.05$, one-way ANOVA). C, The *delt4* and *apx1-2* mutants showed reduced long-lasting ROS signals after treatment with *Pseudomonas syringae* pv. *tomato* (*Pst*) DC3000 (*avrRpt2*). Signals were monitored in the leaf disks for 10 h using a luminol-based chemiluminescent assay after treatment with bacteria ($OD_{600} = 0.03$). The first peak within 1 h is magnified in the upper right corner of the figure. The *rps2* and *rbohD* mutants were used as negative controls. Data are shown as the mean ± SE ($n = 9$). D, Total ROS signals within 1–10 h from (C). Data are shown as the mean ± SE ($n = 9$). Different letters above the bars indicate significant differences between different genotypes ($P \leq 0.05$, one-way ANOVA). E, The *delt4*$^{Dex:avrRpt2}$ leaves showed reduced long-lasting ROS signals after co-treatment with dexamethasone (dex, 10 μM) and flg22 (200 nM). Signals were monitored using a luminol-based chemiluminescent assay in the leaf disks of Col-0$^{Dex:avrRpt2}$ and *delt4*$^{Dex:avrRpt2}$ transgenic plants. Data are shown as the mean ± SE ($n = 18$). F, Total ROS signals after 1 h from (E). Data are shown as the mean ± SE ($n = 18$, $^{****}P \leq 0.0001$, *t* test).

the wild type and *apx1* mutants 3 h after 3-OH-C10:0 treatment. We found that RBOHD accumulation and the phosphorylation of S343/S347 (2 main residues phosphorylated in immunity) in the *delt4* and *apx1-2* mutants were not substantially different from those in the wild type (Figure 3A). *APX1* transcripts were significantly up-regulated at 4, 8, and 12 h after 3-OH-C10:0 treatment (Figure 3B). In *Arabidopsis*, 3-OH-C10:0 is sensed by LIPOOLIGOSACCHARIDE-SPECIFIC REDUCED ELICITATION (LORE), a lectin receptor-like kinase. Treatment with 3-OH-C10:0 did not induce *APX1* up-regulation in *lore* mutants, suggesting that 3-OH-C10:0-triggered *APX1* up-regulation depends on its receptor (Figure 3C). We also examined whether RBOHD is required for 3-OH-C10:0-triggered up-regulation of *APX1* and found that the induction of *APX1* transcripts was significantly reduced in *rbohD* mutants when compared to that in the wild type (Figure 3D). Furthermore, we measured the APX1 protein levels by immunoblotting with an α-cAPX antibody after 3-OH-C10:0 treatment. We found that the APX1 proteins were accumulated 8 and 12 h after treatment (Figure 3E), and the accumulation was reduced in *lore* and *rbohD* mutants (Figure 3, F and G). Notably, the second ROS peak (3–6 h) in response to 3-OH-C10:0 treatment preceded APX1 up-regulation, suggesting that rather than being a prerequisite for ROS production, APX1 up-regulation may be a downstream response to ROS accumulation. Collectively, these results suggest that the reduced long-lasting chemiluminescent signals in *apx1* mutants are not due to the impairment of RBOHD-mediated ROS production.

The *apx1* mutants show increased ROS accumulation, as detected by DAB staining

Avirulent bacteria-induced ROS accumulation could be visualized in leaves by DAB staining, and the presence of H_2O_2 is indicated by a dark-brown precipitate. To relate with the timing of the kinetics of the luminol-emitted light signals, we performed DAB staining 5 h after infiltration with avirulent *Pst* (*avrRpt2*) bacteria. Unfortunately, we did not observe a clear brown color 5 h after bacterial infiltration at an OD_{600} of 0.003. However, a clear brown color was observed 10 h after infiltration with avirulent *Pst* (*avrRpt2*) bacteria, whereas no visible brownness was observed after the control treatment (Figure 4A). The sensitivity of DAB staining is probably weaker than luminol; therefore, we could only detect the accumulated ROS at the end point of ROS production using DAB staining. We then quantified the levels of the brown precipitate using the ImageJ software and found that the *delt4* and *apx1-2* mutants showed color intensity higher than the wild type (Figure 4C). The *rbohD* mutants were used as a negative control to confirm that this brown color was derived from RBOHD-mediated ROS production. The brown precipitates were microscopically observed in the cytosol and associated with the chloroplasts, which were more pronounced in the *apx1* mutants than the wild type (Figure 4B). Consistent with the function of increased ROS levels, *apx1* mutants conferred enhanced resistance to *Pst* (*avrRpt2*) compared with the wild type (Figure 4D). Taken together, these results suggest that *apx1* mutants showed increased ROS accumulation when detected using DAB staining.

APX1 catalyzes luminol oxidation in vitro

The contrasting results obtained between the luminol-based chemiluminescence assay and the DAB staining assay led us to hypothesize that APX1 might be a catalyst for the luminol-H_2O_2 reaction. Luminol reacts with H_2O_2 in the presence of HRP, helping to form 3-aminophthalate (3-APA*), and light is emitted during the decay of the excited-state 3-APA* (Figure 5, A and B). To analyze the catalytic activity of APX1 in luminol-H_2O_2 reaction, APX1 proteins were fused to maltose-binding protein (MBP), and the recombinant proteins were purified from *Escherichia coli*. Compared with MBP alone, MBP-APX1 recombinant proteins significantly enhanced the light emission of the luminol-H_2O_2 reaction (Figure 5B). We then evaluated the enzyme kinetics of APX1 as a catalyst for the luminol-H_2O_2 reaction. Accordingly, in this study, the catalytic activity of APX1 corresponded with the concentrations of luminol (<15 mM) and H_2O_2 (<10 mM) (Figure 5, C and D). High concentrations of H_2O_2 (>10 mM) may inhibit APX1 activity (Figure 5D). Taken together, these results suggest that APX1 can catalyze the oxidation of luminol by H_2O_2 in vitro.

The catalytic mechanism of HRP has been extensively studied using crystallography and site-directed mutagenesis (Savenkova et al., 1998; Martell et al., 2012). Arg38, Phe41, and His42 are critical catalytic residues of HRP that may be involved in heme binding and coordination, and mutations of these residues have a severe impact on peroxidase activity. Compared to HRP, APX1 contains conserved Arg38 and His42 residues, but not Phe41 residue (known as Trp41 in APX1, Figure 5E, Supplemental Figure 10). Therefore, we mutated the Trp41 residue of APX1 to Phe to mimic HRP (referred to as $APX1^{W41F}$). As expected, compared with the wild-type APX1, $APX1^{W41F}$ showed increased catalytic activity in the luminol-H_2O_2 reaction (Figure 5F). However, the R38H mutation of APX1 reduced the light emission of the luminol-H_2O_2 reaction (Figure 5F). Overall, these results suggest that APX1 acts as a peroxidase similar to HRP to catalyze the luminol-H_2O_2 reaction in vitro.

APX1 catalyzes luminol oxidation in vivo

To evaluate whether APX1 acts as a catalyst of luminol in vivo, we transformed $APX1^{W41F}$ and $APX1^{R38H}$ back to *delt4* mutants under the control of the native promoter (Figure 6, A and B). Compared with *pAPX1::APX1/delt4* plants, 4 independent transgenic lines of *pAPX1::*$APX1^{W41F}$*/delt4* displayed significantly increased light intensity in response to *Pst* (*avrRpt2*) when using luminol as a substrate, whereas transgene $APX1^{R38H}$ failed to complement the light intensity of *delt4* (Figure 6, C and 6D). Similar results were observed after LPS treatment (Supplemental Figure 11, A and B).

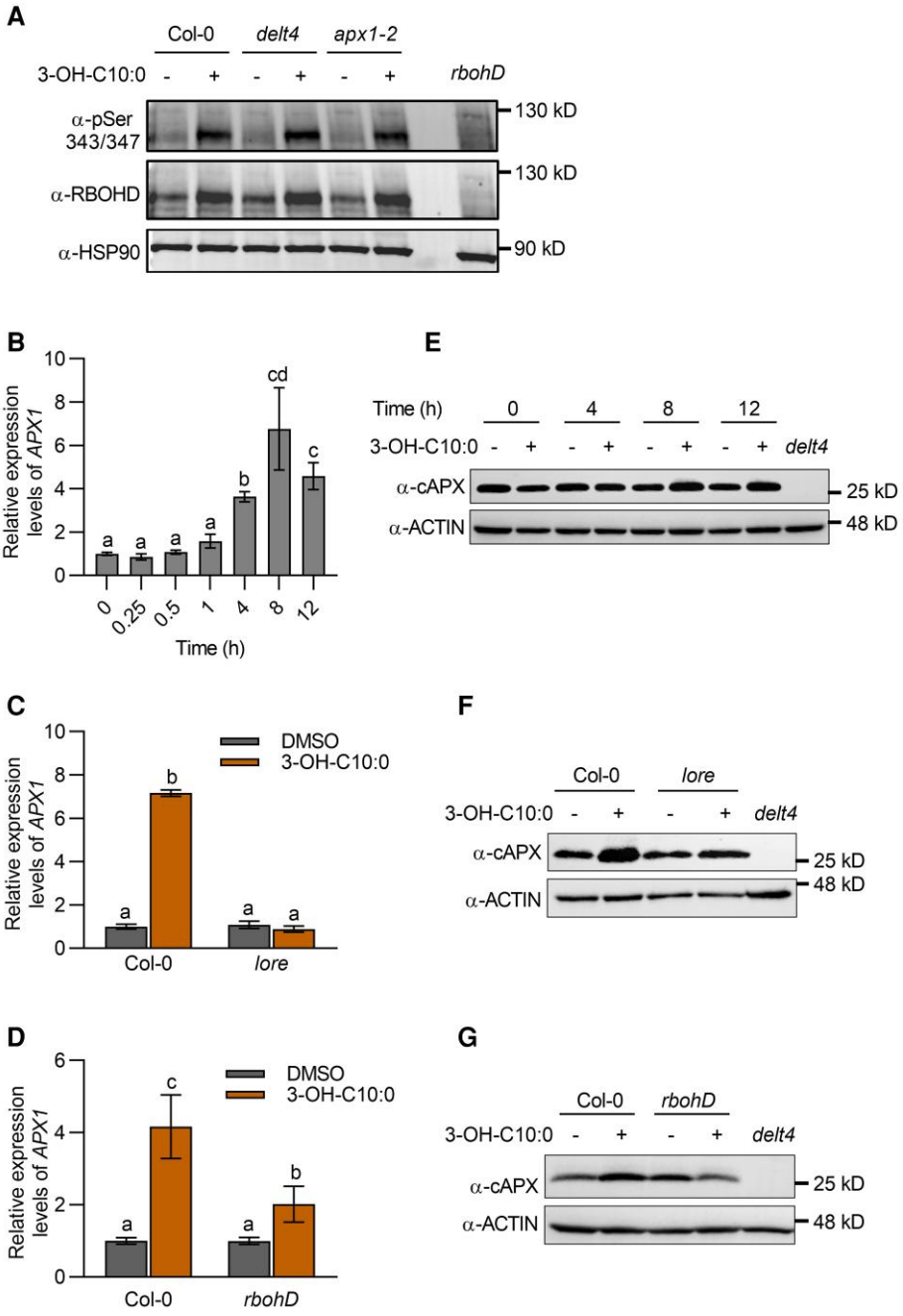

Figure 3 Loss of APX1 does not affect the abundance of RBOHD. A, RBOHD accumulation and phosphorylation after treatment with 3-OH-C10:0 (5 μM). Proteins were detected by immunoblot analysis using α-RBOHD and α-pSer343/347 antibodies, with α-HSP90 used as a loading control. B, *APX1* transcript levels at different time points. Total RNA was prepared at the indicated time points after treatment with 3-OH-C10:0 (5 μM). *APX1* transcript levels were determined using RT-qPCR. Data are shown as the mean ± SE ($n = 3–4$). Different letters above the bars indicate significant differences ($P \leq 0.05$, one-way ANOVA). C, LORE was required for 3-OH-C10:0-triggered up-regulation of *APX1* transcripts. Total RNA was prepared from wild type and *lore* mutants 8 h after treatment with 3-OH-C10:0 (5 μM). Detection of *APX1* transcript levels was similar to that used in (B). Data are shown as the mean ± SE ($n = 3–4$). Different letters above the bars indicate significant differences ($P \leq 0.05$, one-way ANOVA). D, RBOHD contributed to 3-OH-C10:0-triggered up-regulation of *APX1* transcripts. The experimental conditions were similar to those used in (C). Data are shown as the mean ± SE ($n = 3–5$). Different letters above the bars indicate significant differences ($P \leq 0.05$, one-way ANOVA). E, APX1 protein abundance at different time points. Total proteins were extracted at the indicated time points after treatment with 3-OH-C10:0 (5 μM). APX1 protein abundance was detected by immunoblot analysis using an α-cAPX antibody, with α-ACTIN used as a loading control. F, LORE was required for 3-OH-C10:0-triggered APX1 protein accumulation. Total proteins were extracted from wild type and *lore* mutants 8 h after treatment with 3-OH-C10:0 (5 μM). Detection of APX1 protein abundance was similar to that used in (E). G, RBOHD contributed to 3-OH-C10:0-triggered APX1 protein accumulation. The experimental conditions were similar to those used in (F). Experiments for immunoblot analysis in this figure were repeated at least twice with similar trends.

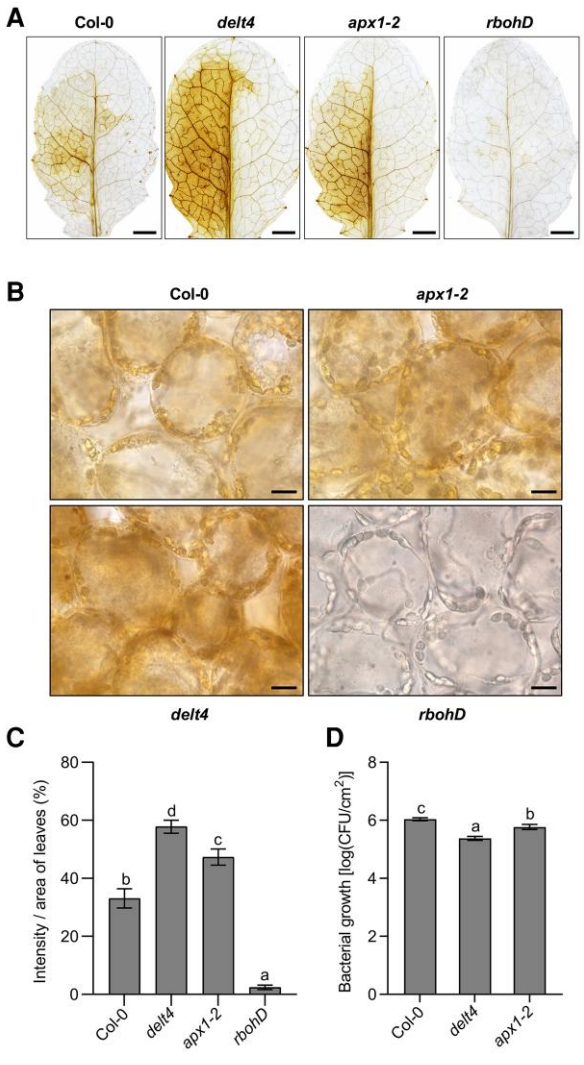

Figure 4 The *apx1* mutants show increased effector-triggered accumulation of ROS, as detected by 3,3′-DAB. A, Images of representative leaves after DAB staining. The seventh to ninth leaves of 4-week-old Col-0, *delt4*, *apx1-2*, and *rbohD* plants were infiltrated with *Pseudomonas syringae* pv. *tomato* (*Pst*) DC3000 (*avrRpt2*) at an OD_{600} of 0.003, with $MgCl_2$ as the control. Bacterial suspensions were infiltrated into the left side of the leaf and the mock control ($MgCl_2$) was into the right side. The leaves were collected 10 h after infiltration and stained with DAB solution. ROS production was visualized as dark-brown precipitates in the detached leaves. Scale bars, 100 μm. B, The subcellular distribution of effector-triggered ROS accumulation. Images were taken from the left half of DAB-stained leaves in (A) under microscopy. Scale bars, 10 μm. C, The intensity of brownness from DAB-stained leaves in (A). DAB staining per unit area of leaves was quantified using the ImageJ software. Data are shown as the mean ± SE ($n = 10$). Different letters above the bars indicate significant differences ($P \leq 0.05$, one-way ANOVA). The experiment was repeated 3 times with similar results. D, *apx1* mutants showed enhanced resistance against *Pst* (*avrRpt2*). Leaves derived from 5-week-old plants with the indicated genotypes were inoculated with *Pst* (*avrRpt2*) at an OD_{600} of 0.0001. The bacterial population in the leaf was determined 3 dpi (day postinoculation). Data are presented as the mean ± SE ($n = 9$). Different letters above the bars indicate significant differences between different genotypes ($P \leq 0.05$, one-way ANOVA).

Collectively, these results further demonstrate that APX1 can catalyze the oxidation of luminol in vivo.

To evaluate whether the APX activity of APX1 contributes to its catalytic activity in the luminol-H_2O_2 reaction, we mutated the Cys32 residue, which is the target for S-nitrosylation and S-sulfhydration and is important for the APX activity (Aroca et al., 2015; Yang et al., 2015). Consistent with previous studies, $APX1^{C32S}$ abolished peroxidase activity using ascorbate as a substrate in vitro (Figure 6E). However, compared with the purified MBP-APX1, MBP-$APX1^{C32S}$ exhibited similar catalytic activity in the in vitro luminol-H_2O_2 system (Figure 6F). Consistently, the transgene $APX1^{C32S}$ complemented the long-lasting luminol-emitted light signals of *delt4* mutants in response to *Pst* (*avrRpt2*) and LPS (Figure 6, G and H, Supplemental Figure 11C). Therefore, these results suggest that APX1 acts as a peroxidase to catalyze the luminol-ROS reaction in vivo, which might be unrelated to its APX activity.

ETI-ROS were observed in the cytosol at later time points, as detected by H_2DCFDA staining

ETI-ROS are produced by RBOHD in the apoplast (Yuan et al., 2021a), but APX1 is known in the cytosol (Panchuk et al., 2002), thus raising a possibility that effectors might also trigger the accumulation of ROS in the cytosol where APX1 catalyzes the luminol oxidation. To test this possibility, we performed H_2DCFDA and AUR staining to measure the temporal and spatial accumulation of ROS in leaves after infiltration with *Pst* (*avrRpt2*) bacteria. H_2DCFDA is a cell-permeable probe that can visualize the apoplastic and cytosolic ROS, while AUR is impermeable to membranes and thus can only probe apoplastic ROS (Ashtamker et al., 2007; Tian et al., 2016). Red and green fluorescent signals were observed in the apoplastic spaces of wild type leaves 4 h after infiltration, as detected by the staining with AUR and H_2DCFDA, respectively (Figure 7A, Supplemental Figure 12). Interestingly, green fluorescent signals in the cytosol began to appear at 6 h and became obvious 8 h after infiltration of *Pst* (*avrRpt2*), whereas fluorescent signals in apoplasts became much weaker at later time points (Figure 7B, Supplemental Figure 12). Furthermore, compared with the wild type, the *apx1* mutants showed stronger apoplastic and intracellular fluorescence signals (Figure 7, Supplemental Figures 12 and 13). Likewise, green fluorescent signals were also observed in the cytosol 4 h after LPS treatment and were largely associated with chloroplasts (Supplemental Figure 14). Collectively, our findings support the notion that ETI-ROS are eventually accumulated in the cytosol.

Discussion

It has been known for a long time that avirulent bacteria trigger a biphasic ROS burst; however, the molecular mechanism underlying the regulation of ETI-ROS and the spatial distribution of ETI-ROS are still unclear. In this study, we found that

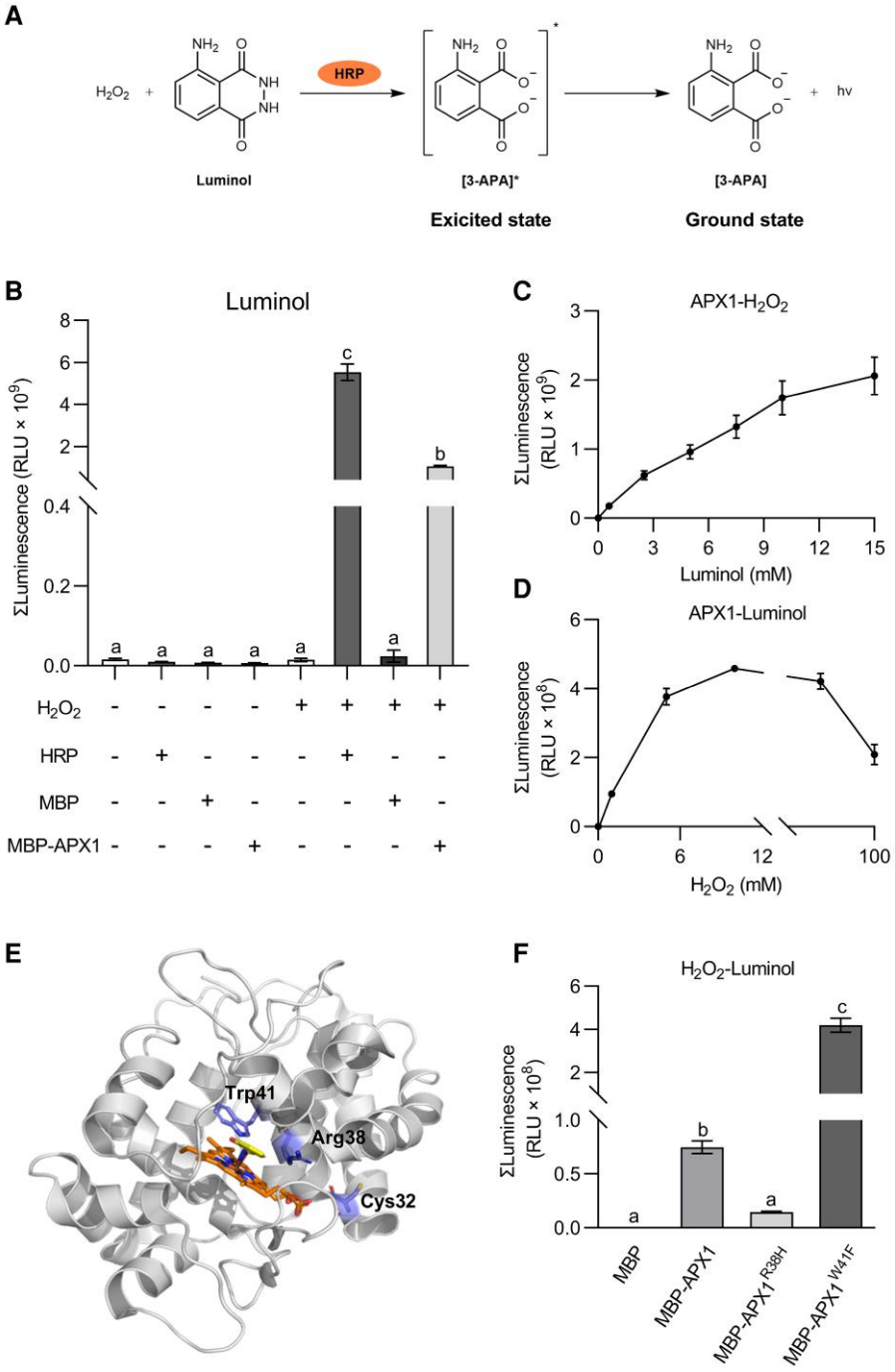

Figure 5 APX1 catalyzes the luminol-H_2O_2 reaction in vitro. A, HRP catalyzes the luminol-H_2O_2 reaction. In the presence of HRP, luminol is oxidized by H_2O_2 to create an excited-state product, 3-aminophthalate (3-APA*), whose decay to the ground state results in photon emission. B, APX1 catalyzed the chemiluminescence reaction of luminol. MBP-tagged APX1 recombinant proteins were purified from *E. coli*. Luminol (300 μM) and MBP, MBP-APX1, or HRP (0.04 mg mL^{-1}) were added first, and light signals were recorded immediately after the addition of H_2O_2 (10 mM). Values represent the total photon counts within 10 min. Data are shown as the mean ± SE ($n = 4$). Different letters above the bars indicate significant differences ($P \leq 0.05$, one-way ANOVA). C, APX1 activity was corresponded with luminol concentrations below 15 mM. Data are shown as the mean ± SE ($n = 5$). D, APX1 activity corresponded with H_2O_2 concentrations below 10 mM. Data are represented as the mean ± SE ($n = 6$). E, Homology modeling of the structure of APX1 using the 3D coordination of the soybean cAPX1 (PDB-1V0H) as a template. The heme cofactor and substrate salicylhydroxamic acid locate in the middle. The 3 important residues, Cys32, Arg38 and Trp41, are marked F, Catalytic abilities of APX1 variants, $APX1^{R38H}$ and $APX1^{W41F}$. Luminol (300 μM) and MBP, MBP-APX1, MBP-$APX1^{R38H}$, or MBP-$APX1^{W41F}$ (0.09 mg mL^{-1}) were added first, and light signals were recorded immediately after the addition of H_2O_2 (1 mM). Values represent the total photon counts within 10 min. Data are shown as the mean ± SE ($n = 8$). Different letters above the bars indicate significant differences ($P \leq 0.05$, one-way ANOVA). All experiments were repeated 3 times with similar results.

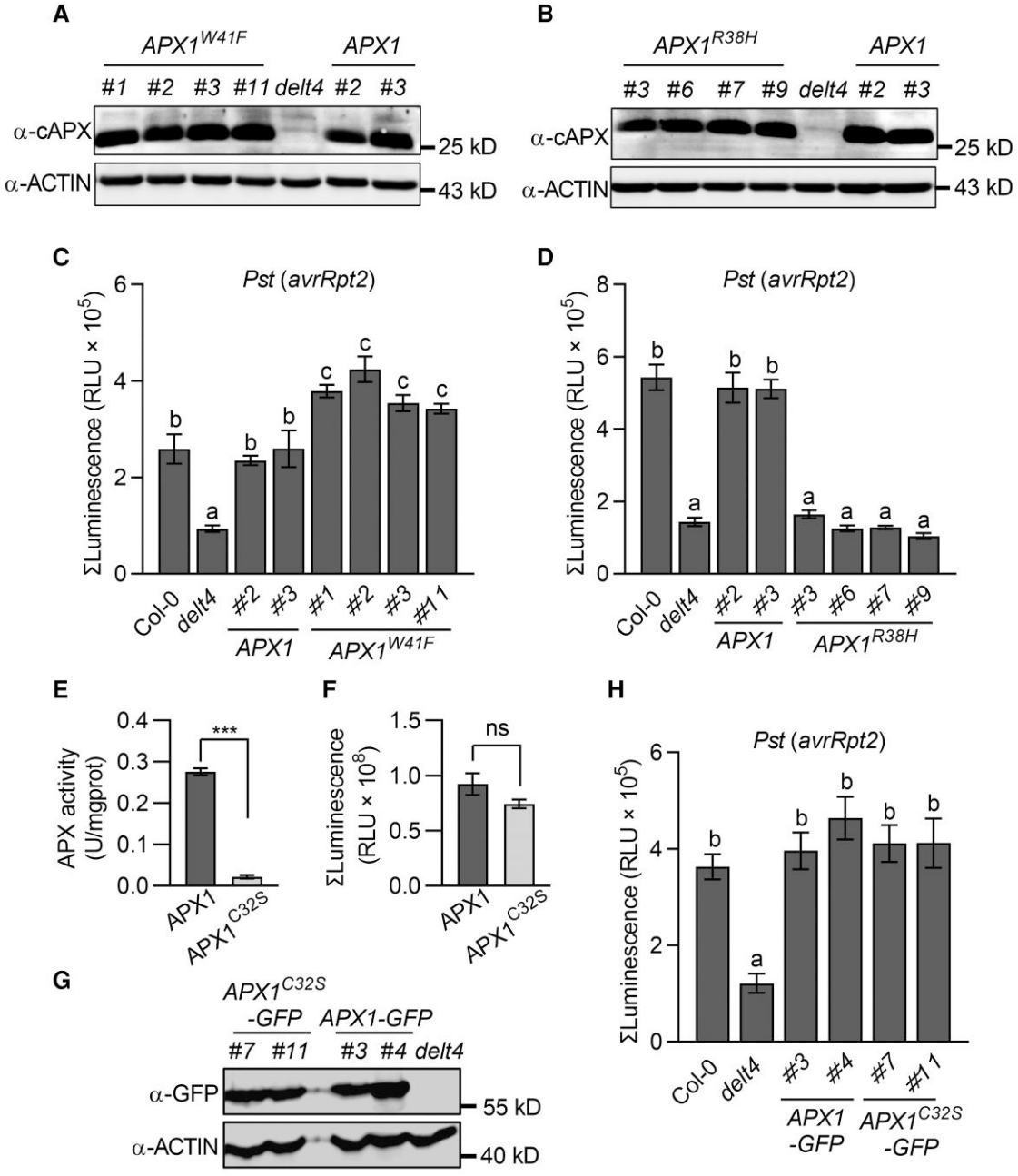

Figure 6 APX1 catalyzes the luminol-H_2O_2 reaction in vivo. A, APX1 protein levels in the 4 independent *pAPX1::APX1*^{W41F}*/delt4* transgenic lines. Total proteins were extracted from 4-week-old leaves and detected by immunoblot analysis using an α-cAPX antibody, with α-ACTIN used as a loading control. B, APX1 protein levels in the 4 independent *pAPX1::APX1*^{R38H}*/delt4* transgenic lines. The experimental conditions were similar to those used in (A). C, Transformation of *APX1*^{W41F} rescued the luminol-emitted long-lasting light signals of *delt4* mutants. Light signals were measured using a luminol-based assay after treatment with *Pseudomonas syringae* pv. *tomato* (*Pst*) DC3000 (*avrRpt2*). The bar graph indicates the total integrated photon counts within 1–10 h after incubation with avirulent bacteria ($OD_{600} = 0.03$). D, Transformation *APX1*^{R38H} failed to complement the luminol-emitted long-lasting light signals of *delt4* mutants in response to *Pst* (*avrRpt2*). The experimental conditions were similar to those used in (C). E, Analysis of the enzymatic activity of MBP-APX1 and MBP-APX1^{C32S} recombinant proteins using ascorbate as a substrate. Data are shown as the mean ± SE ($n = 3$, $^{***}P \leq 0.001$, *t* test). F, Analysis of the enzymatic activity of MBP-APX1 and MBP-APX1^{C32S} recombinant proteins using luminol as a substrate. Values represent the total photon counts within 10 min. Data are shown as the mean ± SE ($n = 7$). Ns stands for no significant differences (*t* test). G, APX1 protein levels in the 2 independent *pAPX1::APX1*^{C32S}*-GFP/delt4* transgenic lines. Total proteins were extracted from 4-week-old leaves and detected by immunoblot analysis using an α-GFP antibody, with α-ACTIN used as a loading control. H, Transformation of *APX1*^{C32S} complemented the luminol-emitted long-lasting light signals of *delt4* mutants in response to *Pst* (*avrRpt2*). The experimental conditions were similar to those used in (C). Data are presented as the mean ± SE ($n = 7$ in C; 10 in D, 8 in H). Different letters above the bars indicate significant differences between different genotypes ($P \leq 0.05$, one-way ANOVA).

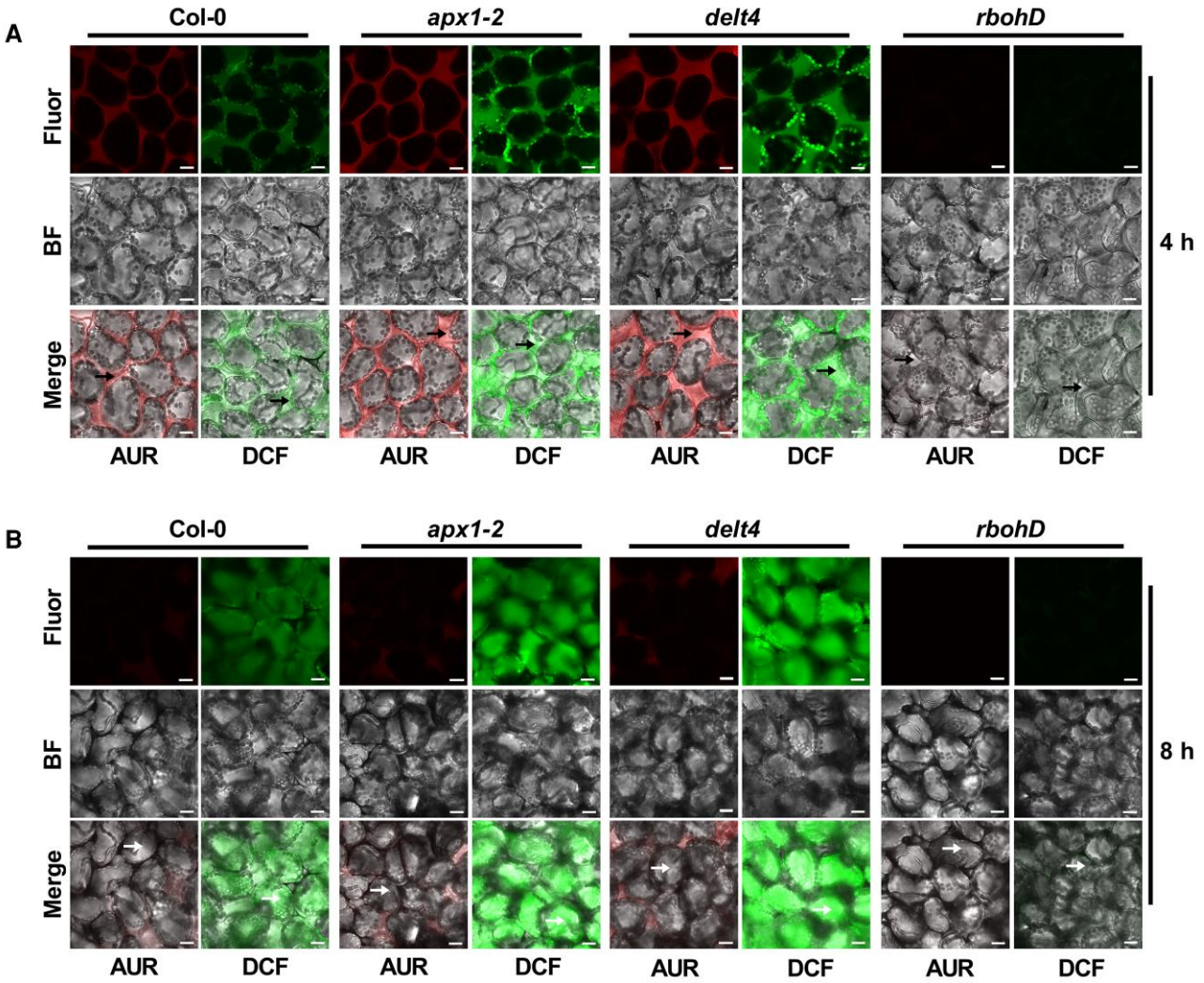

Figure 7 Fluorescence imaging of ROS accumulation in response to avirulent bacteria. ROS accumulation was detected by AUR or H_2DCFDA staining. The abaxial side of 4-week-old leaves from Col-0, *apx1-2*, *delt4*, and *rbohD* plants was infiltrated with *Pst* (*avrRpt2*) at an OD_{600} of 0.03. Fluorescence was observed at 4 (A) and 8 h (B) after bacterial infiltration. Before microscopic observation, leaves were infiltrated with a solution of AUR or H_2DCFDA and incubated for 15–30 min. At least 6 leaves were observed for each treatment, and representative images were shown. Black arrowheads indicate the apoplast space, while white arrowheads indicate the cytoplasm. Scale bars, 15 μm. Fluor, fluorescence; BF, bright field. The experiment was repeated 3 times with similar results.

ETI-ROS were produced in the apoplast at early time points but later accumulated in the cytosol, as detected by H_2DCFDA staining. APX1, a cytosolic protein that normally functions as a ROS scavenger, acts as a catalyst of the luminol-ROS reaction in vitro and in vivo to allow the monitoring of long-lasting ROS accumulation in the cytosol using a luminol-based chemiluminescence assay (Figure 8). Our study provides important insights into the spatial dynamics of ROS accumulation in plant immunity and reveals an unexpected role of APX1 protein in catalyzing luminol-ROS reaction, raising cautions in the detection and interpretation of ROS production widely studied in diverse biological processes of plants.

APXs are characterized by their high specificity to ascorbate, which provides an electron source for detoxifying H_2O_2 in the cytosol (Raven, 2003). However, previous studies suggest that APXs may also play other roles besides scavenging toxic H_2O_2. The APXs in *Brachypodium distachyon* and Arabidopsis can serve as coumarate 3-hydroxylases (C3H) involved in the early steps of lignin biosynthesis that catalyzes the 3-hydroxylation of 4-coumarate to caffeate (Barros et al., 2019). Rice (*Oryza sativa*) APX2 and Arabidopsis APX1 proteins have been found to function as chaperone molecules (Hong et al., 2018; Kaur et al., 2021). Moreover, APX1 might show peroxidase activity toward other aromatic electron donors, which is unrelated to its physiological functions; for example, an engineered ascorbate peroxidase (APEX2) has been successfully used for electron microscopic imaging in mammalian cells (Lam et al., 2015; Martell et al., 2017). This technique was developed based

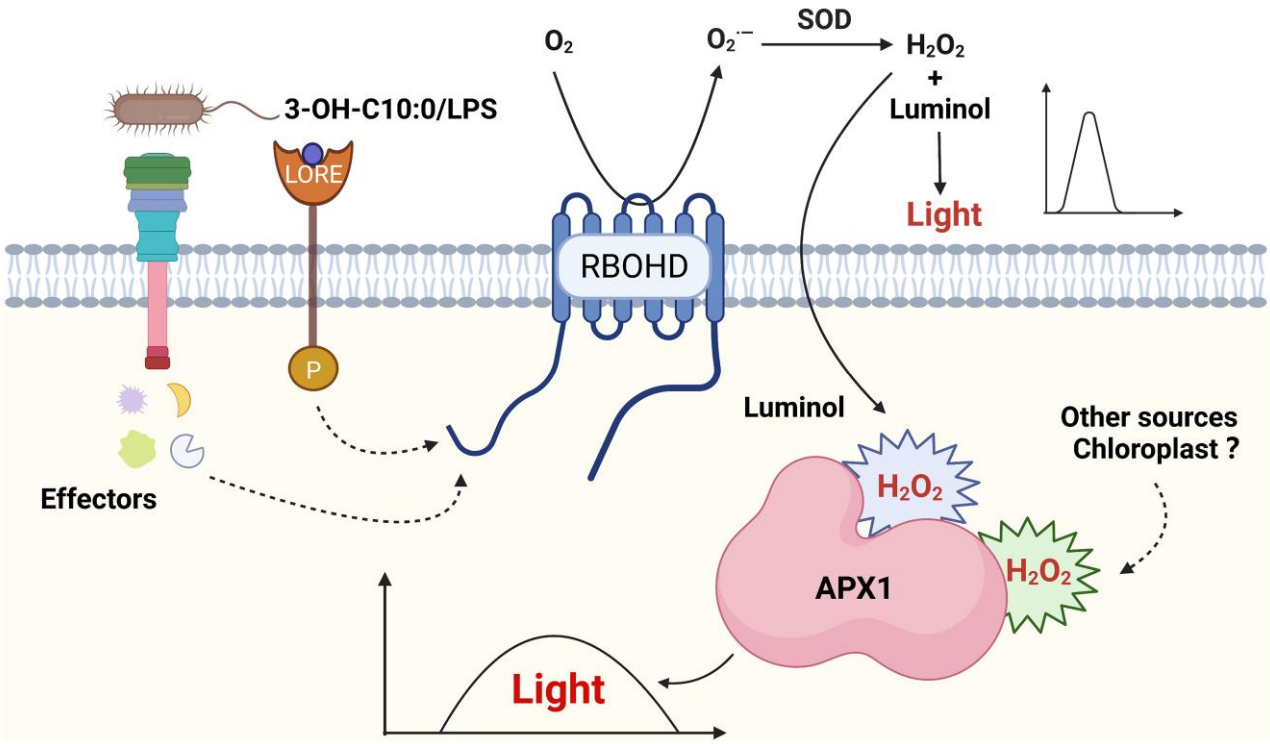

Figure 8 A schematic model illustrating APX1-mediated monitoring of the kinetics of long-lasting production of ROS in the cytosol. LPS, 3-OH-C10:0, or bacterial effectors trigger a long-lasting ROS burst in the cytosol. When ROS production is monitored by a luminol-based chemiluminescence assay, cytosolic APX1 serves as a catalyst for luminol oxidation. The model was created with BioRender.com.

on the function of HRP in catalyzing DAB and Amplex UltraRed as substrates. However, HRP requires posttranslational modification and is not active in the cytosol, thus limiting its use in vivo (Porstmann et al., 1985). Unlike HRP, APX1 is naturally active in the cytosol; therefore, it was chosen as an HRP mimic for labeling cytosolic proteins in mammalian cells (Lam et al., 2015; Martell et al., 2017). However, in this study, the in vivo APX1 may not be required for DAB staining in Arabidopsis when measuring H_2O_2 production. The *apx1* mutants did not show a decrease in brown precipitates after infiltration with *Pst* (*avrRpt2*) strain, suggesting that Arabidopsis may contain other peroxidases that show higher catalytic activity toward DAB than APX1 does. Instead, in this study, APX1 showed catalytic activity toward luminol and that APX1^{W41F}, the most HRP-like mutant that can facilitate the incorporation of aromatic residues into the active site, displayed higher catalytic activity toward the luminol substrate than that displayed by wild-type APX1. Likewise, APEX2, which contains a W41F mutation in APX1, has been developed because of its high activity toward the DAB substrate in mammalian cells (Lam et al., 2015; Martell et al., 2017). Therefore, we believe that the catalytic activity of APX1 toward luminol provides important information that may help to engineer a cytosolic peroxidase that allows real-time monitoring of intracellular ROS production without interfering with the biological ROS levels in mammalian cells.

Many methods have been developed for ROS detection, including chemiluminescent probes, colorimetric dyes, fluorescent dyes, $CeCl_3$ staining, and genetically encoded biosensors. Each has advantages and potential limitations (Dikalov et al., 2007; Griendling et al., 2016; Mamone et al., 2016; Zhang et al., 2018). Among these methods, fluorescent dyes, $CeCl_3$ staining, and genetically encoded biosensors can measure subcellular ROS production. However, the limitations include nonspecific fluorescence, labor-intensive protocols, or the requirement for transgenic plants (Zulfugarov et al., 2011). Colorimetric dyes are relatively easier to use and do not require other instruments but show high levels of nonspecific staining (as they react with any redox molecules). The luminol-based chemiluminescence assay for detecting biological ROS production has several advantages. The biggest advantage of this assay is the real-time detection of ROS kinetics, as the emission of light can be monitored every second by a photon detector or a CCD camera (Khan et al., 2014; Yang et al., 2020). In addition, luminol-based chemiluminescence assays have higher sensitivity compared to other probes and are less expensive than fluorescent probes and $CeCl_3$ (Kim et al., 2019). This method is also suitable for large-scale genetic mutant screens because it can be set up in a 96-well plate (Smith and Heese, 2014). Luminol-based chemiluminescence assays have been successfully used to isolate mutants defective in flg22-induced ROS bursts and to identify several important signaling components in response

to PAMPs (Boutrot et al., 2010; Macho et al., 2012; Li et al., 2019, 2021; Wu et al., 2022). In this study, we found that APX1 acts as an intracellular peroxidase that catalyzes the oxidation of luminol and allows the use of a luminol-based chemiluminescence assay to monitor intracellular ROS production. However, more attention should be paid when this method is used. Because APX1 is an H_2O_2-scavenging enzyme, a lack of APX1 would yield higher H_2O_2 levels in the cytosol. If APX1 is impaired during a luminol-based chemiluminescence assay to monitor intracellular ROS production, researchers may draw wrong conclusions regarding the actual intracellular ROS levels. To avoid this, it is advisable to use other methods to confirm the results of experiments using this method.

ETI-ROS were also found to be accumulated in the cytosol by $CeCl_3$ staining (Hamdoun et al., 2013). We monitored the temporal and spatial accumulation of ROS by H_2DCFDA staining after infiltration with an avirulent bacterial strain and found that ROS were produced in the apoplast, but accumulated in the cytosol at later time points. The accumulation of ETI-ROS in the cytosol could be partially due to the translocation of H_2O_2 from the apoplast into the cytosol. It has been suggested that biomembrane channels (aquaporins) could mediate the transmembrane diffusion of H_2O_2 during immune signaling (Bienert and Chaumont, 2014; Tian et al., 2016; Rodrigues et al., 2017). However, we could not rule out the possibility that RBOHD-mediated early ROS signaling may be conveyed to the intracellular environment, which is a prerequisite for inducing other ROS sources, such as chloroplasts, mitochondria, and peroxisomes, which then release ROS into the cytosol (Asada, 2006; de Torres Zabala et al., 2015; Mignolet-Spruyt et al., 2016; Sun et al., 2018). Moreover, apoplastic ROS might induce a secondary signal, such as calcium influx into the cells, and thus induce a second long-lasting ROS burst (Ogasawara et al., 2008; Kimura et al., 2012; Gilroy et al., 2016). In addition, RBOHD is prone to be endocytosed and the endocytosed RBOHD may still function in producing superoxide in the cytosol. Indeed, this mechanism has been found in mammals. For example, the NADPH oxidase NOX1 is endocytosed to generate ROS within smooth muscle cells in response to TNF-α (Miller et al., 2010). Recently, in *Arabidopsis*, endocytosis of RBOHD was also found to be necessary for salt-induced ROS production in roots (Lee et al., 2022), and salt stress could trigger intracellular ROS accumulation (Lin et al., 2006; Xie et al., 2011; Ben Rejeb et al., 2015; Petrov et al., 2015; Mao et al., 2018; Jin et al., 2021), suggesting that RBOHD might be endocytosed to produce ROS in the cytosol after salt treatment. Nevertheless, how the ETI-ROS were accumulated into the cytosol require further investigation.

In conclusion, ETI-ROS were accumulated in the cytosol, and APX1 catalyzes the luminol-ROS reaction, allowing the measurement of the kinetics of intracellular ROS production using a luminol-based approach.

Materials and methods

Plant materials and growth conditions

Seeds of the Arabidopsis (*Arabidopsis thaliana*) *rbohD* (CS9555), *lore* (Sail_857_E06), *cat2-2* (Salk_057998), *cat3* (Salk_092911), and *rps2* (101C) mutants were obtained from the Arabidopsis Biological Resource Center (Ohio State University, USA). Seeds of the Arabidopsis *apx1-2* (Salk_000249), *apx2-1* (Salk_091880), and *apx2-2* (Salk_057686) mutants were obtained from the Non-Profit Arabidopsis Share Center (https://www.arashare.cn/). The Arabidopsis $rps2^{Dex:avrRpt2}$ transgenic plants were kindly provided by Prof. Jun Liu at the China Agricultural University. The Arabidopsis Col-$0^{Dex:avrRpt2}$ and $delt4^{Dex:avrRpt2}$ transgenic plants were obtained from F_2 segregating progenies by crossing $rps2^{Dex:avrRpt2}$ plants with Col-0 and *delt4* plants, respectively. For young seedling assays, the seeds were sterilized with 10% (v/v) sodium hypochlorite and grown on half-strength Murashige-Skoog agar plates in a growth chamber (model A1000AR, Conviron, Manitoba, Canada) under a 16 h photoperiod, 75% humidity, and 22°C. For mature plant assays, 10-day-old seedlings were transferred to pots containing a peat-based compost (Sun Gro Horticulture, Agawam, MA, USA) and grown under a 14-h photoperiod for ROS assays or a 8-h photoperiod for bacterial growth assays.

Map-based cloning of the *DELT4* gene

The *delt4* mutant in the Col-0 background was isolated, as previously described (Li et al., 2021). To generate a mapping population, the *delt4* mutant was crossed with the Landsberg *erecta* (Ler) ecotype, and individuals with reduced ROS production after LPS treatment were isolated from the F_2 generation. Genomic DNA was extracted from each individual for linkage analysis. The PCR markers were developed using the Arabidopsis Mapping Platform (https://www.arabidopsis.org/browse/Cereon/help.jsp), and the primers used are listed in Supplemental Table 1.

Next-generation sequencing from bulked-segregant analysis

The *delt4* mutant was backcrossed to Col-0, and the generated F_1 progeny was self-pollinated to produce F_2 seeds. Individuals with or without ROS production after LPS treatment were pooled separately and subjected to whole-genome sequencing using the Illumina X-ten system (Gene Denovo Biotechnology, Guangzhou, China). Illumina short reads generated from the bulked DNA samples were cleaned and filtered according to their Phred quality score and aligned against the public wild-type reference genome using the Burrows-Wheeler Aligner software (Li and Durbin, 2009). Alignment files were converted to sequence alignment map/binary alignment map files using SAMtools (Li et al., 2009). A sliding window analysis was applied to the frequency distribution of SNPs (SNP-index) in the population of bulked individuals. The Δ(SNP-index) values

were calculated by subtracting the SNP-index values between the 2 bulk pools.

Plasmid construction and generation of transgenic plants

All the primers used for gene cloning in this study are listed in Supplemental Table 1. The coding or genomic sequences of the indicated genes were amplified and cloned into a pDONR-Zeo plasmid via BP cloning (Thermo Fisher Scientific, Waltham, MA, USA). The inserts were verified by sequencing and cloned into the destination plasmids via LR cloning (Thermo Fisher Scientific). PCR-based site-directed mutagenesis was used to construct plasmids with point mutations in a gene of interest. All constructs used for the generation of transgenic plants were verified by sequencing and are listed in Supplemental Table 2. Each resulting construct was introduced into *Agrobacterium tumefaciens* strain GV3101, and the *Agrobacterium*-mediated floral dip method was used to generate transgenic Arabidopsis plants.

RNA isolation and reverse transcription quantitative PCR (RT-qPCR)

Total RNA was extracted from 8-day-old seedlings using an *Easy* Plant RNA kit (Easy-Do, Hangzhou, China) according to the manufacturer's instructions. First-strand complementary DNA (cDNA) was synthesized from 1 μg of isolated RNA using HiScript II reverse transcriptase (Vazyme Biotech, Nanjing, China). RT-qPCR reactions were performed using an SYBR Green Master Mix (Vazyme Biotech). The relative levels of gene expression were calculated using the $2^{-\Delta\Delta Ct}$ method with *ELONGATION FACTOR1α* (*EF1α*) as an internal control. All primers used for the RT-qPCR are listed in Supplemental Table 1.

Expression and purification of recombinant proteins

The recombinant proteins were expressed and purified as previously described (Li et al., 2021). *APX1* cDNA was cloned into pMAL-c2x-GW (gateway) vectors, and the resulting plasmid was transformed into *E. coli* BL21. All constructs used for prokaryotic expression were verified by sequencing and are listed in Supplemental Table 2. The bacterial cultures were grown in liquid Luria-Bertani medium at 37°C for approximately 3 h. When the optical density at 600 nm (OD_{600}) reached approximately 0.8–1.0, 0.2 mM of isopropyl-β-D-thiogalactoside was added to induce the expression of MBP-tagged APX1. The cultures were collected 6 h after induction, and MBP-tagged recombinant proteins were purified using amylose resin (New England Biolabs, Ipswich, MA, USA) following the manufacturer's instructions.

Protein extraction and immunoblot analysis

Detection of RBOHD using immunoblot analysis was performed as previously described (Li et al., 2021). To detect APX1, total proteins were extracted with a buffer containing 50 mM Tris–HCl (pH 8.0), 150 mM NaCl, 1% Triton X-100 (v/v), and 1× protease inhibitor cocktail (Merck KGaA, Darmstadt, Germany). The extracted proteins were separated by 12% SDS-polyacrylamide gel electrophoresis and transferred onto polyvinylidene difluoride membranes (Merck KGaA). Proteins were detected with an α-cAPX antibody (Agrisera, Vännäs, Sweden) and an α-ACTIN antibody (ABclonal, Wuhan, China).

ROS detection by luminol-based chemiluminescent assay

ROS detection by luminol-based chemiluminescence assay was performed as previously described, with some modifications (Liang et al., 2013). Leaf disks (0.2 cm^2) were obtained from the seventh to ninth leaves of 4-week-old plants and incubated overnight with water in a 96-well plate. The following day, 600 μM luminol (Merck KGaA) was added along with the indicated elicitors, including LPS (L9143, Merck KGaA), flg22 (GenScript, Nanjing, China), 3-OH-C10:0 (Bide Pharmatech Ltd., Shanghai, China), and dexamethasone (MedChemExpress, Monmouth Junction, NJ, USA). The chemiluminescent signal was immediately recorded using a Photek camera (HRPCS5, Photek, East Sussex, UK). When bacteria were used for the luminol-based assay, the bacterial cells were freshly diluted to the desired concentration as previously described (Smith and Heese, 2014). HRP (Merck KGaA) was exogenously applied for the luminol-based assay at 20 mg L^{-1} (w/v).

ROS detection by histochemical DAB staining

DAB staining was performed as described previously, with some modifications (Shang-Guan et al., 2018). The seventh to ninth leaves of 4-week-old plants were infiltrated with *Pst* (*avrRpt2*) at an OD_{600} of 0.003. The leaves were detached 10 h post infiltration, vacuum-infiltrated with DAB staining solution (1 mg mL^{-1}, pH 6.0), and incubated at 24°C room temperature for 2 h. Chlorophyll was removed by incubation with glacial acetic acid/glycerol/ethanol (1:1:3), and the dark-brown colored leaves (visualizing the generation of H_2O_2) were observed under a light microscope (Nikon, Japan). The intensity of DAB staining per unit area of leaves was quantified using the ImageJ software (https://imagej.nih.gov/ij/).

ROS detection by fluorescent staining

AUR and H_2DCFDA staining were performed as described previously, with some modifications (Tian et al., 2016; Yuan et al., 2021a). The seventh to ninth leaves of 4-week-old plants were infiltrated with *Pst* (*avrRpt2*) (OD_{600} = 0.03) or LPS (100 μg mL^{-1}). For bacterial infiltration, leaves were directly infiltrated with a solution of 10 μM AUR (Merck KGaA) or 10 μM H_2DCFDA (MedChemExpress) and incubated for 10–30 min; for LPS treatment, leaves were detached and incubated with an H_2DCFDA solution (10 μM) for 30 min.

Images were captured under an Olympus FV3000 confocal laser scanning microscope with the following setting of laser/detection wavelength: oxidized H_2DCFDA (488/500–540), oxidized AUR (561/565–620), and chlorophyll autofluorescence (640/650–750). The laser transmissivity was set as 0.2% in all fluorescence detection.

Bacterial growth assay

For disease assay, *Pst* (*avrRpt2*) was cultured in a selective King's B (KB) medium overnight at 28°C to an OD_{600} of 0.8–1.0. Bacteria were collected by centrifugation and resuspended with 10 mM $MgCl_2$ and the concentration was adjusted to an OD_{600} of 0.0001. Using a needleless syringe, the resuspended bacterial solution was infiltrated into the abaxial surfaces of 5-week-old *Arabidopsis* leaves. After being air-dried in the plant growth room, the inoculated plants were covered with a transparent plastic dome for at least 6 h to maintain a high humidity for disease to develop. For quantification at 3 dpi, 3 leaf discs from 3 different leaves were collected with an 8-mm-diameter cork borer (with disc area of 0.502 cm^2) as 1 biological repeat, and 9 repeats were taken for each genotype. Samples were ground and diluted in 10 mM $MgCl_2$, and the extraction solutions were then plated on selective KB medium plates (100 µL per plate). The number of colonies was counted 36 h after incubation at 28°C, and bacterial growth was represented as CFU/cm^2 of leaf tissue.

Measurement of APX activity

APX activity was measured as previously described with some modifications (Nakano and Asada, 1981). Briefly, the reaction mixture contained 25 mM PBS (pH = 7.0) with 0.1 mM EDTA, 0.5 mM ascorbate, 2 mM H_2O_2, and 100 µg purified proteins (MBP-APX1 and MBP-APX1^{C32S}). After the initiation of the reaction by adding H_2O_2. the samples were immediately analyzed with Tecan Spark Multimode Microplate Reader by measuring the absorbance at A_{290} every 5 s for a 2-min recording time. Protein concentration was determined with Coomassie Brilliant Blue G-250 according to the method of Bradford using bovine serum albumin as the standard.

Examination of the ultrastructure of leaf chloroplasts by transmission electron microscopy

Small fragments (approximately 3 mm^2) were excised from freshly harvested leaves of 4-week-old mature plants with a razor blade, and then immediately transferred to a cold fixation buffer [2.5% glutaraldehyde (v/v) in 0.1 M phosphate buffer, pH 7.0]. After incubation with the fixation buffer for at least 4 h, the samples were washed 3 times for 15 min in phosphate buffer (0.1 M, pH 7.0), postfixed for 1–2 h with 1% osmium tetroxide (w/v) in phosphate buffer, and washed again 3 times with phosphate buffer. The doubled-fixed samples were then dehydrated, infiltrated, embedded, sectioned, and stained for observation as described previously (Bestwick et al., 1995). The sections were examined using a transmission electron microscope (H7650, Hitachi, Tokyo, Japan) at an accelerating voltage of 75 kV.

Confocal microscopy observation of SSU-GFP

Transgenic plants expressing SSU-GFP were used as previously described (Shang-Guan et al., 2018). The GFP signals were detected under a confocal microscope (FV3000, Olympus, Tokyo, Japan) with the same parameters as oxidized H_2DCFDA.

Modeling the structure of APX1

Sequences were aligned using the freely available web server, ESPript 3.0 (http://espript.ibcp.fr; Robert and Gouet, 2014). Homology modeling of the structure of the APX1 molecule was performed using the 3D coordination of the soybean (*Glycine max*) cAPX1 (PDB-1V0H) as the template. The images were generated using PyMol (http://pymol.sourceforge.net).

Statistical analysis

The statistical analyses were performed by 2-tailed Student's *t* test with Office Excel software for paired comparison or by one-way analysis of variance (ANOVA) with SPSS software for multiple comparisons. Groups or samples with statistically significant differences are marked with asterisk(s) ($^*P \leq 0.05$; $^{**}P \leq 0.01$; $^{***}P \leq 0.001$, $^{****}P \leq 0.0001$, Student's *t* test) or different letters ($P \leq 0.05$, one-way ANOVA, lowercase letters). Each experiment was repeated at least 3 times and data were represented as the mean ± SE as indicated.

Accession numbers

Sequence data from this article can be found in the GenBank/EMBL data libraries under accession numbers_: *APX1* (At1g07890), *RBOHD* (At5g47910), *LORE* (At1g61380), *RPS2* (At4g26090), *APX2* (At3g09640), *APX6* (At4g32320), *CAT1* (At1g20630), *CAT2* (At4g35090), *CAT3* (At1g20620), *GPX1* (At2g25080), *GPX2* (At2g31570), *GPX3* (At2g43350), *GPX7* (At4g31870) and *avrRpt2* from *P. syringae* (Q6LAD6).

Supplemental data

The following materials are available in the online version of this article.

Supplemental Figure S1. The kinetics of ROS burst triggered by LPS/3-OH-C10:0/*Pst* (*avrRpt2*).

Supplemental Figure S2. HRP is not indispensable when ROS level is high enough to oxidize luminol.

Supplemental Figure S3. Molecular characterization of the *DELT4* gene.

Supplemental Figure S4. *APX1* transcripts and protein abundance in *apx1* mutants.

Supplemental Figure S5. The *apx1* mutants show reduced effector-triggered long-lasting luminescent signals.

Supplemental Figure S6. The exogenous addition of HRP cannot restore the reduced ETI-ROS signals in *apx1* mutants.

Supplemental Figure S7. Expression of genes involved in ROS scavenging.

Supplemental Figure S8. *apx2*, *cat2*, and *cat3* mutants are not impaired in LPS-triggered long-lasting ROS accumulation.

Supplemental Figure S9. Chloroplasts of *delt4* mutants are not impaired after LPS treatment.

Supplemental Figure S10. Sequence alignment of APX1 with horseradish peroxidase (HRP) and soybean peroxidase (SBP).

Supplemental Figure S11. Effect of *APX1* mutation on luminol-based light signals triggered by LPS.

Supplemental Figure S12. The temporal and spatial ETI-ROS detected by H_2DCFDA staining.

Supplemental Figure S13. Detection of ROS accumulation in leaves infiltrated with $MgCl_2$ by AUR and H_2DCFDA staining.

Supplemental Figure S14. *apx1* mutants show increased cytosolic ROS accumulation after LPS treatment, as detected by H_2DCFDA staining.

Supplemental Table S1. Primers used in this study.

Supplemental Table S2. Constructs used in this study.

Acknowledgments

We thank Prof. Jun Liu (China Agricultural University, China) for kindly providing *rps2*$^{Dex:avrRpt2}$ seeds, Xiao-xiao Feng (Agricultural Experiment Station of Zhejiang University) for her assistance with plant growth, and Prof. Yanni Yin (Zhejiang University, China) for her discussion of the manuscript.

Funding

This work was supported by the Key Research and Development Program of Zhejiang Province (2021C02064-7, 2021C02009, and 2022C02016) and National Natural Science Foundation of China (31622006 and 31970279). Xiu-Fang Xin was supported by the Chinese Academy of Sciences Strategic Priority Research Program (type-B; grant number XDB27040211). Minhang Yuan was supported by National Postdoctoral Program for Innovative Talents (BX2021313) and Shanghai Postdoctoral Excellence Program.

Conflict of interest statement. The authors declare that they have no conflict of interest.

References

Apel K, Hirt H (2004) Reactive oxygen species: metabolism, oxidative stress, and signal transduction. Annu Rev Plant Biol **55**(1): 373–399

Aroca A, Serna A, Gotor C, Romero LC (2015) S-sulfhydration: a cysteine posttranslational modification in plant systems. Plant Physiol **168**(1): 334–342

Asada K (2006) Production and scavenging of reactive oxygen species in chloroplasts and their functions. Plant Physiol **141**(2): 391–396

Ashtamker C, Kiss V, Sagi M, Davydov O, Fluhr R (2007) Diverse subcellular locations of cryptogein-induced reactive oxygen species production in tobacco bright yellow-2 cells. Plant Physiol **143**(4): 1817–1826

Baker CJ, Orlandi EW (1995) Active oxygen in plant pathogenesis. Annu Rev Phytopathol **33**(1): 299–321

Barros J, Escamilla-Trevino L, Song L, Rao X, Serrani-Yarce JC, Palacios MD, Engle N, Choudhury FK, Tschaplinski TJ, Venables BJ, et al. (2019) 4-Coumarate 3-hydroxylase in the lignin biosynthesis pathway is a cytosolic ascorbate peroxidase. Nat Commun **10**(1): 1994

Baxter A, Mittler R, Suzuki N (2014) ROS as key players in plant stress signalling. J Exp Bot **65**(5): 1229–1240

Ben Rejeb K, Benzarti M, Debez A, Bailly C, Savouré A, Abdelly C (2015) NADPH oxidase-dependent H_2O_2 production is required for salt-induced antioxidant defense in *Arabidopsis thaliana*. J Plant Physiol **174**: 5–15

Bestwick CS, Bennett MH, Mansfield JW (1995) Hrp mutant of *Pseudomonas syringae* pv. *phaseolicola* induces cell wall alterations but not membrane damage leading to the hypersensitive reaction in lettuce. Plant Physiol **108**(2): 503–516

Bienert GP, Chaumont F (2014) Aquaporin-facilitated transmembrane diffusion of hydrogen peroxide. Biochim Biophys Acta **1840**(5): 1596–1604

Bigeard J, Colcombet J, Hirt H (2015) Signaling mechanisms in pattern-triggered immunity (PTI). Mol Plant **8**(4): 521–539

Boller T, Felix G (2009) A renaissance of elicitors: perception of microbe-associated molecular patterns and danger signals by pattern-recognition receptors. Annu Rev Plant Biol **60**(1): 379–406

Boutrot F, Segonzac C, Chang KN, Qiao H, Ecker JR, Zipfel C, Rathjen JP (2010) Direct transcriptional control of the Arabidopsis immune receptor FLS2 by the ethylene-dependent transcription factors EIN3 and EIL1. Proc Natl Acad Sci U S A **107**(32): 14502–14507

Brandes RP, Weissmann N, Schröder K (2014) Nox family NADPH oxidases: molecular mechanisms of activation. Free Radic Biol Med **76**: 208–226

Camejo D, Guzmán-Cedeño Á, Moreno A (2016) Reactive oxygen species, essential molecules, during plant-pathogen interactions. Plant Physiol Biochem **103**: 10–23

Caverzan A, Passaia G, Rosa SB, Ribeiro CW, Lazzarotto F, Margis-Pinheiro M (2012) Plant responses to stresses: role of ascorbate peroxidase in the antioxidant protection. Genet Mol Biol **35**(4 Suppl 1): 1011–1019

Chandra S, Martin GB, Low PS (1996) The Pto kinase mediates a signaling pathway leading to the oxidative burst in tomato. Proc Natl Acad Sci U S A **93**(23): 13393–13397

Coyle PM, Thorpe GH, Kricka LJ, Whitehead TP (1986) Enhanced luminescent quantitation of horseradish peroxidase conjugates: application in an enzyme immunoassay for digoxin. Ann Clin Biochem **23**(1): 42–46

Davletova S, Rizhsky L, Liang H, Shengqiang Z, Oliver DJ, Coutu J, Shulaev V, Schlauch K, Mittler R (2005) Cytosolic ascorbate peroxidase 1 is a central component of the reactive oxygen gene network of *Arabidopsis*. Plant Cell **17**(1): 268–281

de Torres Zabala M, Littlejohn G, Jayaraman S, Studholme D, Bailey T, Lawson T, Tillich M, Licht D, Bolter B, Delfino L, et al. (2015) Chloroplasts play a central role in plant defence and are targeted by pathogen effectors. Nat Plants **1**(6): 15074

Dikalov S, Griendling KK, Harrison DG (2007) Measurement of reactive oxygen species in cardiovascular studies. Hypertension **49**(4): 717–727

Doke N (1983) Involvement of superoxide anion generation in the hypersensitive response of potato-tuber tissues to infection with an incompatible race of *Phytophthora infestans* and to the hyphal wall components. Physiol Plant Pathol **23**(3): 345–357

Gest N, Gautier H, Stevens R (2013) Ascorbate as seen through plant evolution: the rise of a successful molecule? J Exp Bot **64**(1): 33–53

Gilroy S, Białasek M, Suzuki N, Górecka M, Devireddy AR, Karpiński S, Mittler R (2016) ROS, calcium, and electric signals: key mediators of rapid systemic signaling in plants. Plant Physiol **171**(3): 1606–1615

Griendling KK, Touyz RM, Zweier JL, Dikalov S, Chilian W, Chen YR, Harrison DG, Bhatnagar A, American Heart Association Council on Basic Cardiovascular S (2016) Measurement of reactive oxygen species, reactive nitrogen species, and redox-dependent signaling in the cardiovascular system: a scientific statement from the American Heart Association. Circ Res **119**(5): e39–e75

Großkinsky DK, Koffler BE, Roitsch T, Maier R, Zechmann B (2012) Compartment-specific antioxidative defense in Arabidopsis against virulent and avirulent *Pseudomonas syringae*. Phytopathology **102**(7): 662–673

Hamdoun S, Liu Z, Gill M, Yao N, Lu H (2013) Dynamics of defense responses and cell fate change during Arabidopsis-*Pseudomonas syringae* interactions. PLoS One **8**(12): e83219

Hong SH, Tripathi BN, Chung MS, Cho C, Lee S, Kim JH, Bai HW, Bae HJ, Cho JY, Chung BY, et al. (2018) Functional switching of ascorbate peroxidase 2 of rice (OsAPX2) between peroxidase and molecular chaperone. Sci Rep **8**(1): 9171

Jiang L, Chen Z, Gao Q, Ci L, Cao S, Han Y, Wang W (2016) Loss-of-function mutations in the *APX1* gene result in enhanced selenium tolerance in *Arabidopsis thaliana*. Plant Cell Environ **39**(10): 2133–2144

Jin J, Li K, Qin J, Yan L, Wang S, Zhang G, Wang X, Bi Y (2021) The response mechanism to salt stress in Arabidopsis transgenic lines over-expressing of GmG6PD. Plant Physiol Biochem **162**: 74–85

Jones JD, Dangl JL (2006) The plant immune system. Nature **444-**(7117): 323–329

Joo JH, Wang S, Chen JG, Jones AM, Fedoroff NV (2005) Different signaling and cell death roles of heterotrimeric G protein α and β subunits in the Arabidopsis oxidative stress response to ozone. Plant Cell **17**(3): 957–970

Kadota Y, Liebrand TWH, Goto Y, Sklenar J, Derbyshire P, Menke FLH, Torres MA, Molina A, Zipfel C, Coaker G, et al. (2019) Quantitative phosphoproteomic analysis reveals common regulatory mechanisms between effector- and PAMP-triggered immunity in plants. New Phytol **221**(4): 2160–2175

Kadota Y, Shirasu K, Zipfel C (2015) Regulation of the NADPH oxidase RBOHD during plant immunity. Plant Cell Physiol **56**(8): 1472–1480

Kadota Y, Sklenar J, Derbyshire P, Stransfeld L, Asai S, Ntoukakis V, Jones JD, Shirasu K, Menke F, Jones A, et al. (2014) Direct regulation of the NADPH oxidase RBOHD by the PRR-associated kinase BIK1 during plant immunity. Mol Cell **54**(1): 43–55

Kaur S, Prakash P, Bak DH, Hong SH, Cho C, Chung MS, Kim JH, Lee S, Bai HW, Lee SY, et al. (2021) Regulation of dual activity of ascorbate peroxidase 1 from *Arabidopsis thaliana* by conformational changes and posttranslational modifications. Front Plant Sci **12**: 678111

Khan P, Idrees D, Moxley MA, Corbett JA, Ahmad F, von Figura G, Sly WS, Waheed A, Hassan MI (2014) Luminol-based chemiluminescent signals: clinical and non-clinical application and future uses. Appl Biochem Biotechnol **173**(2): 333–355

Kim JS, Jeong K, Murphy JM, Rodriguez YAR, Lim SS (2019) A quantitative method to measure low levels of ROS in nonphagocytic cells by using a chemiluminescent imaging system. Oxid Med Cell Longev **2019**: 1754593

Kimura S, Kaya H, Kawarazaki T, Hiraoka G, Senzaki E, Michikawa M, Kuchitsu K (2012) Protein phosphorylation is a prerequisite for the Ca^{2+}-dependent activation of Arabidopsis NADPH oxidases and may function as a trigger for the positive feedback regulation of Ca^{2+} and reactive oxygen species. Biochim Biophys Acta **1823**(2): 398–405

Koussevitzky S, Suzuki N, Huntington S, Armijo L, Sha W, Cortes D, Shulaev V, Mittler R (2008) Ascorbate peroxidase 1 plays a key role in the response of *Arabidopsis thaliana* to stress combination. J Biol Chem **283**(49): 34197–34203

Kutschera A, Dawid C, Gisch N, Schmid C, Raasch L, Gerster T, Schaffer M, Smakowska-Luzan E, Belkhadir Y, Vlot AC, et al. (2019) Bacterial medium-chain 3-hydroxy fatty acid metabolites trigger immunity in *Arabidopsis* plants. Science **364**(6436): 178–181

Lam SS, Martell JD, Kamer KJ, Deerinck TJ, Ellisman MH, Mootha VK, Ting AY (2015) Directed evolution of APEX2 for electron microscopy and proximity labeling. Nat Methods **12**(1): 51–54

Lamb C, Dixon RA (1997) The oxidative burst in plant disease resistance. Annu Rev Plant Physiol Plant Mol Biol **48**(1): 251–275

Lee J, Hanh Nguyen H, Park Y, Lin J, Hwang I (2022) Spatial regulation of RBOHD via AtECA4-mediated recycling and clathrin-mediated endocytosis contributes to ROS accumulation during salt stress response but not flg22-induced immune response. Plant J **109**(4): 816–830

Levine A, Tenhaken R, Dixon R, Lamb C (1994) H_2O_2 from the oxidative burst orchestrates the plant hypersensitive disease resistance response. Cell **79**(4): 583–593

Li H, Durbin R (2009) Fast and accurate short read alignment with burrows-wheeler transform. Bioinformatics **25**(14): 1754–1760

Li H, Handsaker B, Wysoker A, Fennell T, Ruan J, Homer N, Marth G, Abecasis G, Durbin R, Genome Project Data Processing S (2009) The sequence alignment/map format and SAMtools. Bioinformatics **25**(16): 2078–2079

Li QY, Li P, Myint Phyu Sin Htwe N, Shangguan KK, Liang Y (2019) Antepenultimate residue at the C-terminus of NADPH oxidase RBOHD is critical for its function in the production of reactive oxygen species in *Arabidopsis*. J Zhejiang Univ Sci B **20**(9): 713–727

Li L, Li M, Yu L, Zhou Z, Liang X, Liu Z, Cai G, Gao L, Zhang X, Wang Y, et al. (2014) The FLS2-associated kinase BIK1 directly phosphorylates the NADPH oxidase RbohD to control plant immunity. Cell Host Microbe **15**(3): 329–338

Li P, Zhao L, Qi F, Htwe N, Li Q, Zhang D, Lin F, Shang-Guan K, Liang Y (2021) The receptor-like cytoplasmic kinase RIPK regulates broad-spectrum ROS signaling in multiple layers of plant immune system. Mol Plant **14**(10): 1652–1667

Liang Y, Cao Y, Tanaka K, Thibivilliers S, Wan J, Choi J, Kang C, Qiu J, Stacey G (2013) Nonlegumes respond to rhizobial Nod factors by suppressing the innate immune response. Science **341**(6152): 1384–1387

Lin J, Wang Y, Wang G (2006) Salt stress-induced programmed cell death in tobacco protoplasts is mediated by reactive oxygen species and mitochondrial permeability transition pore status. J Plant Physiol **163**(7): 731–739

Ma S, Lapin D, Liu L, Sun Y, Song W, Zhang X, Logemann E, Yu D, Wang J, Jirschitzka J, et al. (2020) Direct pathogen-induced assembly of an NLR immune receptor complex to form a holoenzyme. Science **370**(6521):eabe3069

Macho AP, Boutrot F, Rathjen JP, Zipfel C (2012) Aspartate oxidase plays an important role in Arabidopsis stomatal immunity. Plant Physiol **159**(4): 1845–1856

Mamone L, Di Venosa G, Sáenz D, Batlle A, Casas A (2016) Methods for the detection of reactive oxygen species employed in the identification of plant photosensitizers. Methods **109**: 73–80

Mao C, Ding J, Zhang B, Xi D, Ming F (2018) OsNAC2 positively affects salt-induced cell death and binds to the OsAP37 and OsCOX11 promoters. Plant J **94**(3): 454–468

Martell JD, Deerinck TJ, Lam SS, Ellisman MH, Ting AY (2017) Electron microscopy using the genetically encoded APEX2 tag in cultured mammalian cells. Nat Protoc **12**(9): 1792–1816

Martell JD, Deerinck TJ, Sancak Y, Poulos TL, Mootha VK, Sosinsky GE, Ellisman MH, Ting AY (2012) Engineered ascorbate peroxidase as a genetically encoded reporter for electron microscopy. Nat Biotechnol **30**(11): 1143–1148

Mignolet-Spruyt L, Xu E, Idänheimo N, Hoeberichts FA, Mühlenbock P, Brosché M, Van Breusegem F, Kangasjärvi J (2016) Spreading the news: subcellular and organellar reactive oxygen species production and signalling. J Exp Bot **67**(13): 3831–3844

Miller FJ, Chu X, Stanic B, Tian X, Sharma RV, Davisson RL, Lamb FS (2010) A differential role for endocytosis in receptor-mediated activation of Nox1. Antioxid Redox Signal **12**(5): 583–593.

Mittler R (2002) Oxidative stress, antioxidants and stress tolerance. Trends Plant Sci **7**(9): 405–410

Mittler R (2017) ROS are good. Trends Plant Sci **22**(1): 11–19
Mittler R, Vanderauwera S, Suzuki N, Miller G, Tognetti VB, Vandepoele K, Gollery M, Shulaev V, Van Breusegem F (2011) ROS signaling: the new wave? Trends Plant Sci **16**(6): 300–309
Mur LA, Lloyd AJ, Cristescu SM, Harren FJ, Hall MA, Smith AR (2009) Biphasic ethylene production during the hypersensitive response in Arabidopsis: a window into defense priming mechanisms? Plant Signal Behav **4**(7): 610–613
Nakano Y, Asada K (1981) Hydrogen peroxide is scavenged by ascorbate specific peroxidase in spinach chloroplasts. Plant Cell Physiol **22**(5): 867–880
Ngou BPM, Ahn HK, Ding P, Jones JDG (2021) Mutual potentiation of plant immunity by cell-surface and intracellular receptors. Nature **592**(7852): 110–115
Ogasawara Y, Kaya H, Hiraoka G, Yumoto F, Kimura S, Kadota Y, Hishinuma H, Senzaki E, Yamagoe S, Nagata K, et al. (2008) Synergistic activation of the *Arabidopsis* NADPH oxidase AtrbohD by Ca^{2+} and phosphorylation. J Biol Chem **283**(14): 8885–8892
Panchuk II, Volkov RA, Schöffl F (2002) Heat stress- and heat shock transcription factor-dependent expression and activity of ascorbate peroxidase in Arabidopsis. Plant Physiol **129**(2): 838–853
Pandey S, Fartyal D, Agarwal A, Shukla T, James D, Kaul T, Negi YK, Arora S, Reddy MK (2017) Abiotic stress tolerance in plants: myriad roles of ascorbate peroxidase. Front Plant Sci **8**: 581
Petrov V, Hille J, Mueller-Roeber B, Gechev TS (2015) ROS-mediated abiotic stress-induced programmed cell death in plants. Front Plant Sci **6**: 69
Porstmann B, Porstmann T, Nugel E, Evers U (1985) Which of the commonly used marker enzymes gives the best results in colorimetric and fluorimetric enzyme immunoassays: horseradish peroxidase, alkaline phosphatase or β-galactosidase? J Immunol Methods **79**(1): 27–37
Qi Y, Tsuda K, Glazebrook J, Katagiri F (2011) Physical association of pattern-triggered immunity (PTI) and effector-triggered immunity (ETI) immune receptors in Arabidopsis. Mol Plant Pathol **12**(7): 702–708
Qi J, Wang J, Gong Z, Zhou JM (2017) Apoplastic ROS signaling in plant immunity. Curr Opin Plant Biol **38**: 92–100
Raven EL (2003) Understanding functional diversity and substrate specificity in haem peroxidases: what can we learn from ascorbate peroxidase? Nat Prod Rep **20**(4): 367–381
Robert X, Gouet P (2014) Deciphering key features in protein structures with the new ENDscript server. Nucleic Acids Res **42**(W1): W320–W324
Rodrigues O, Reshetnyak G, Grondin A, Saijo Y, Leonhardt N, Maurel C, Verdoucq L (2017) Aquaporins facilitate hydrogen peroxide entry into guard cells to mediate ABA- and pathogen-triggered stomatal closure. Proc Natl Acad Sci U S A **114**(34): 9200–9205
Sang Y, Macho AP (2017) Analysis of PAMP-triggered ROS burst in plant immunity. Methods Mol Biol **1578**: 143–153
Savenkova MI, Kuo JM, Ortiz de Montellano PR (1998) Improvement of peroxygenase activity by relocation of a catalytic histidine within the active site of horseradish peroxidase. Biochemistry **37**(30): 10828–10836
Shang-Guan K, Wang M, Htwe N, Li P, Li Y, Qi F, Zhang D, Cao M, Kim C, Weng H, et al. (2018) Lipopolysaccharides trigger two successive bursts of reactive oxygen species at distinct cellular locations. Plant Physiol **176**(3): 2543–2556
Shigeoka S, Ishikawa T, Tamoi M, Miyagawa Y, Takeda T, Yabuta Y, Yoshimura K (2002) Regulation and function of ascorbate peroxidase isoenzymes. J Exp Bot **53**(372): 1305–1319
Shigeoka S, Maruta T (2014) Cellular redox regulation, signaling, and stress response in plants. Biosci Biotechnol Biochem **78**(9): 1457–1470
Smirnoff N (2000) Ascorbic acid: metabolism and functions of a multifacetted molecule. Curr Opin Plant Biol **3**(3): 229–235
Smirnoff N, Wheeler GL (2000) Ascorbic acid in plants: biosynthesis and function. Crit Rev Biochem Mol Biol **35**(4): 291–314
Smith JM, Heese A (2014) Rapid bioassay to measure early reactive oxygen species production in *Arabidopsis* leave tissue in response to living *Pseudomonas syringae*. Plant Methods **10**(1): 6
Sun M, Jiang F, Cen B, Wen J, Zhou Y, Wu Z (2018) Respiratory burst oxidase homologue-dependent H_2O_2 and chloroplast H_2O_2 are essential for the maintenance of acquired thermotolerance during recovery after acclimation. Plant Cell Environ **41**(10): 2373–2389
Suzuki N, Koussevitzky S, Mittler R, Miller G (2012) ROS and redox signalling in the response of plants to abiotic stress. Plant Cell Environ **35**(2): 259–270
Thorpe GH, Kricka LJ (1986) Enhanced chemiluminescent reactions catalyzed by horseradish peroxidase. Methods Enzymol **133**: 331–353
Tian S, Wang X, Li P, Wang H, Ji H, Xie J, Qiu Q, Shen D, Dong H (2016) Plant aquaporin AtPIP1; 4 links apoplastic H_2O_2 induction to disease immunity pathways. Plant Physiol **171**(3): 1635–1650
Torres MA, Dangl JL, Jones JD (2002) *Arabidopsis* gp91^{phox} homologues *AtrbohD* and *AtrbohF* are required for accumulation of reactive oxygen intermediates in the plant defense response. Proc Natl Acad Sci USA **99**(1): 517–522
Wang J, Hu M, Wang J, Qi J, Han Z, Wang G, Qi Y, Wang HW, Zhou JM, Chai J (2019) Reconstitution and structure of a plant NLR resistosome conferring immunity. Science **364**(6435):eaav5870
Wu B, Li P, Hong X, Xu C, Wang R, Liang Y (2022) The receptor-like cytosolic kinase RIPK activates NADP-malic enzyme 2 to generate NADPH for fueling ROS production. Mol Plant **15**(5): 887–903
Xie YJ, Xu S, Han B, Wu MZ, Yuan XX, Han Y, Gu Q, Xu DK, Yang Q, Shen WB (2011) Evidence of Arabidopsis salt acclimation induced by up-regulation of *HY1* and the regulatory role of RbohD-derived reactive oxygen species synthesis. Plant J **66**(2): 280–292
Yang M, Huang J, Fan J, Du J, Pu K, Peng X (2020) Chemiluminescence for bioimaging and therapeutics: recent advances and challenges. Chem Soc Rev **49**(19): 6800–6815
Yang H, Mu J, Chen L, Feng J, Hu J, Li L, Zhou JM, Zuo J (2015) S-nitrosylation positively regulates ascorbate peroxidase activity during plant stress responses. Plant Physiol **167**(4): 1604–1615
Yuan M, Jiang Z, Bi G, Nomura K, Liu M, Wang Y, Cai B, Zhou JM, He SY, Xin XF (2021a) Pattern-recognition receptors are required for NLR-mediated plant immunity. Nature **592**(7852): 105–109
Yuan M, Ngou BPM, Ding P, Xin XF (2021b) PTI-ETI crosstalk: an integrative view of plant immunity. Curr Opin Plant Biol **62**: 102030
Zhang YF, Dai MH, Yuan ZH (2018) Methods for the detection of reactive oxygen species. Anal Methods **10**(38): 4625–4638
Zipfel C (2014) Plant pattern-recognition receptors. Trends Immunol **35**(7): 345–351
Zulfugarov IS, Tovuu A, Kim J-H, Lee C-H (2011) Detection of reactive oxygen species in higher plants. J Plant Biol **54**(6): 351–357